Monte Carlo Simulation of 3-D Buffered Ca^{2+} Diffusion in Neuroendocrine Cells

Amparo Gil, Javier Segura, José A. G. Pertusa, and Bernat Soria
Instituto de Bioingeniería, Universidad Miguel Hernández, 03202 Elche, Alicante, Spain

ABSTRACT Buffered Ca^{2+} diffusion in the cytosol of neuroendocrine cells is a plausible explanation for the slowness and latency in the secretion of hormones. We have developed a Monte Carlo simulation to treat the problem of 3-D diffusion and kinetic reactions of ions and buffers. The 3-D diffusion is modeled as a random walk process that follows the path of each ion and buffer molecule, combined locally with a stochastic treatment of the first-order kinetic reactions involved. Such modeling is able to predict [Ca^{2+}] and buffer concentration time courses regardless of how low the calcium influx is, and it is therefore a convenient method for dealing with physiological calcium currents and concentrations. We study the effects of the diffusional and kinetic parameters of the model on the concentration time courses as well as on the local equilibrium of buffers with calcium. An in-mobile and fast endogenous buffer as described by Klingauf and Neher (1997, *Biophys. J.* 72:674–690) was able to reach local equilibrium with calcium; however, the exogenous buffers considered are displaced drastically from equilibrium at the start of the calcium pulse, particularly below the pores. The versatility of the method also allows the effect of different arrangements of calcium channels on submembrane gradients to be studied, including random distribution of calcium channels and channel clusters. The simulation shows how the particular distribution of channels or clusters can be of relevance for secretion in the case where the distribution of release granules is correlated with the channels or clusters.

INTRODUCTION

Ca^{2+}-triggered secretion by neuroendocrine cells is known to be a relatively slow process and with longer latencies when compared with the secretion of neurotransmitters in synapses (Augustine et al., 1985; Llinás et al., 1981). In chromaffin cells, for instance, it is known that secretion continues during tens of milliseconds after a short pulse (Chow et al., 1992). In pancreatic β-cells, latency between elevation of [Ca^{2+}] and exocytosis has recently been reported (Eliasson et al., 1997).

A plausible explanation for such slow mechanisms of secretion may be found in the existence of cytosolic buffers that delay the response by slowing down the free calcium transient. The way in which Ca^{2+} exogenous chelators interfere with secretion, in both chromaffin (Chow et al., 1996) and β-cells (Bokvist et al., 1995; Pertusa et al., submitted for publication), strongly supports such a possibility.

Speaking in general terms, one can summarize the basic ingredients of calcium signaling (Clapham, 1995) in neuroendocrine cells as consisting of transient of calcium ions through the cell membrane, uptake and release of Ca^{2+} by internal stores, diffusion of calcium, and binding/unbinding by endogenous (or exogenously added) buffers. When secretion is studied, the dynamics of the release granules responsible for secretion as well as their spatial distribution also have to be taken into account.

Several studies have previously considered the problem of buffered calcium diffusion in excitable cells, modeling the system by means of diffusion-reaction differential equations, solved numerically using finite differences schemes (Sala and Hernández-Cruz, 1990; Nowycky and Pinter, 1993; Klingauf and Neher, 1997). Other approaches, to mathematically simplify the models, considered different kinds of approximations valid either for rapid buffers (Wagner and Keizer, 1994; Smith et al., 1996) or in the linear regime (Naraghi and Neher, 1997). Such previous studies addressed the importance of the study of Ca^{2+}-buffered diffusion both to gain insight into the secretory response (Klingauf and Neher, 1997) as well as to correctly interpret data from fluorescence experiments (Nowycky and Pinter, 1993; Smith et al., 1996) that use exogenous buffers as indicators of Ca^{2+} intracellular activities.

In this study we have adopted a Monte Carlo method to model the buffered diffusion of calcium. Monte Carlo simulations have been previously used successfully to study reaction and diffusion processes in biological systems (Saxton, 1994, 1996; Riley et al., 1995; Kruk et al., 1997). Our motivations for adopting such a scheme are several. First, no a priori assumptions about the symmetry of the problem are needed to reduce the number of spatial dimensions; in this way, we can perform a three-dimensional simulation of diffusion. Second, the boundary conditions of the problem are more easily taken into account, and one can vary such conditions with ease. For instance, with a Monte Carlo simulation it is a simple task to model the entrance of ions through channel pores (not necessarily regularly distributed) and to consider the possibility of clustered channels. Third,

Received for publication 19 January 1999 and in final form 19 October 1999.

Address reprint requests to Dr. Javier Segura, Departamento de Ciencias, Experimentales y Tecnologia Edificio La Galia, Universidad Miguel Hernández, 03202 Elche, Alicante, Spain. Tel.: 34-966-658-626; Fax: 34-966-658-793; E-mail: segura@flamenco.ific.uv.es.

0006-3495/00/01/13/21 $2.00

Monte Carlo techniques are robust methods for solving complex problems in which different agents come into play together, interacting among themselves. The robustness and versatility of the method enable us to safely study tendencies when the parameters affected by large uncertainties are varied, which is indeed the case of the diffusional and kinetic parameters of our system. Last, but not least: as we shall see, given the relatively small number of Ca^{2+} ions and buffer molecules involved, a stochastic approach to the problem may be more appropriate and safer than the solution of the reaction-diffusion differential equations (in terms of concentrations).

METHODS

We have built a Monte Carlo simulation to treat the problem of 3-D diffusion and kinetic reactions of calcium ions and buffers. The main ingredients of the simulation are

1. Selection of the geometrical configuration and distribution of channel pores
2. Selection of initial concentrations
3. Diffusion of Ca^{2+} and mobile buffers
4. Binding and unbinding of Ca^{2+} ions by buffers
5. Entry of Ca^{2+} through channel pores

One can also consider extrusion mechanisms through the membrane (Sala and Hernández-Cruz, 1990; Klingauf and Neher, 1997); however, the contribution to Ca^{2+} concentration profiles for time intervals smaller than 100 ms seems to be irrelevant (Sala and Hernández-Cruz, 1990). Other phenomena not considered in the present simulation are the effect of obstacles (release granules, mitochondria) in diffusion (Saxton, 1994; Ölveczky and Verckman, 1998), sequestration, and release by internal stores (like mitochondria—see Xu et al., 1997; or granules, sarcoplasmic reticulum, etc.). In the present study we limited our field of investigation to the problem of buffered calcium diffusion in a subdomain with uniformly (but not necessarily regularly) distributed calcium channels (or channel clusters), with a Ca^{2+} influx discretized in space (the entry is restricted to the pores).

Let us now discuss the different ingredients of the simulation of Ca^{2+}-buffered diffusion and how the sequence of the simulation works.

Geometrical configuration

The only a priori geometrical simplification considered in our study, to save computational time, is the restriction to a conical subdomain of the whole cell, assuming zero flux on the lateral boundaries of the cone. This is a reasonable approximation if one assumes that the conical subdomain (which, typically, will have from 15 to 45 channel pores) is embedded in a larger submembrane region where the channels are more or less uniformly distributed. In such a case, one can always find, approximately, a conical boundary with zero flux. When a spherical cell with uniformly distributed channels is considered, the conical section should reach the center of the cell.

The selection of such a geometrical configuration considerably relaxes the assumption of symmetry around a channel pore assumed by Klingauf and Neher (1997) and thus allows us to consider randomly but uniformly distributed channels or channel clusters, not necessarily regularly distributed.

We take a conical section with $R = 5\ \mu$m of depth and a base with radius $r = 1\ \mu$m (Fig. 1), and we assume that the net flux of ions and mobile buffer molecules is zero on the lateral side of the cone. The conical section would reach the center of a typical pancreatic β-cell. We approximate the spherical cell membrane by a plane surface (upper side of the cone), discarding negligible curvature effects (its surface increases by only 1% when curvature is considered).

A 3-D and orthogonal grid mapping the conical section is considered, with length of the sides $\Delta l = 0.105\ \mu$m (see Fig. 1). The total number of cubic compartments is 4450, 253 of which are located at the upper slice of the cone (submembrane domain); the number decreases until the greatest depth is reached, at the vertex of the cone, where there is only one compartment.

On the upper side of the cone we distribute the channel pores uniformly and randomly. Because of the assumption of symmetry needed to balance the number of ions on the fictitious walls of the conical subdomain, the distribution of channels (or channel clusters) should preferably not break the (approximate) uniformity in the surface distribution.

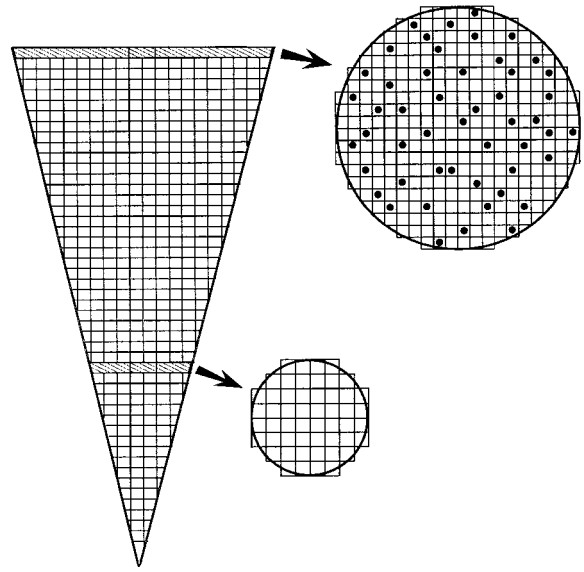

FIGURE 1 Conical domain considered for the simulation. The dots represent the calcium channels.

The typical number of calcium channel pores ranges from 15 to 45, corresponding to a density of channels ranging from 5 to 15 pores per μm^2, which seems to be in the range of physiological values (Klingauf and Neher, 1997).

Notice that when a cell of radius $R = 5$ μm with uniformly distributed calcium channels is considered, the relation between the whole-cell current (I_{wc}) and the incoming current for our conical domain (I_d) is given by the ratio of the surface of the submembrane domain over the surface of the whole cell, that is, $I_d/I_{wc} = r^2/(2R)^2 = 10^{-2}$. In our simulations, we always refer to the domain current (I_d); the whole-cell current would be a factor 100 larger in the situation described.

Diffusion

The 3-D diffusion of ions and mobile buffers is modeled as a random walk process. During every time step Δt and for each dimension, a particle has a 50% chance of remaining in its initial position and a 25% chance of moving in either the positive or the negative direction.

The time step corresponding to such probabilities is given by the relation (Kruk et al., 1997)

$$\Delta t = (\Delta l)^2/4D = 12.5\ \mu s, \qquad (1)$$

where $D = 220$ $\mu m^2/s$ the diffusion coefficient for Ca^{2+} in cytoplasm (Allbritton et al., 1992). To model 3-D diffusion we have to take into account the probability of staying in the same cubic compartment of the grid and the probabilities of moving to the surrounding 26 cubic compartments (Fig. 2). After each diffusional time interval Δt we decide the fate of each ion with the probabilities of staying or moving in each compartment of the grid as described in Fig. 2.

Depending on the mobile buffer considered (EGTA, Fura-2, etc.), the corresponding diffusion coefficient can be typically about two to five times smaller than that for Ca^{2+}, so that the characteristic diffusion times are about two to five times bigger. Thus the diffusion of buffer particles can be simulated by moving them in exactly the same way that Ca^{2+} ions are moved, but only after two to five simulation steps (Kruk et al., 1997). By simply tuning the probabilities of staying or moving for the buffer particles we could also account for noninteger ratios of diffusion coefficients; however, given the considerable uncertainties in the actual values of diffusion coefficients in cytoplasm (Klingauf and Neher, 1997), considering integer ratios seems to be enough.

Typically, the total number of buffer molecules per compartment in our simulations is as "large" as 300. Thus to save time it is convenient not to select the next position of each of them, but to redistribute the bulk of buffer particles according to the probabilities of going to the different 27 positions (see Fig. 2). When we have $N > 64$ buffer particles to diffuse, we take $N = 64c + R$, with $R < 64$ (c and R are integers). Then we consider the "bulk" diffusion of the $64c$ buffer particles according to the following distribution:

c buffer particles for each corner of the cube
$2c$ buffer particles for each middle point of an edge
$4c$ buffer particles for each center of a side
$8c$ buffer particles in the center of the cube,

and we decide probabilistically the position of the remaining R particles according to the probabilities in Fig. 2.

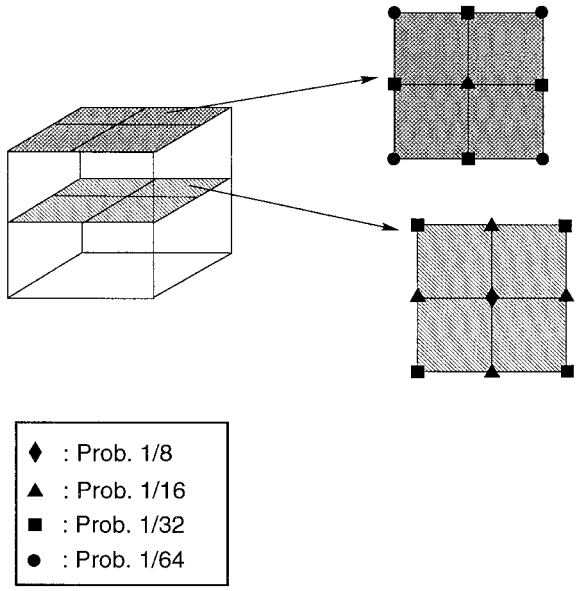

FIGURE 2 Probabilities for a particle in the center of the cube (corresponding to a given compartment of the grid) of staying in this same compartment or moving to a neighbor compartment in a 3-D random walk step. Notice that each vertex, middle point of an edge, center of a side, or center of the cube in the diagram corresponds to a given cubic compartment of the grid.

For the free calcium ions, given the number of incoming ions and the moderate expected rise of free calcium (for instance, for 10 μM there are seven ions per compartment in average), the bulk redistribution is absent on most occasions and only the probabilistic selection comes into play. This fact suggests that, for the size of the grid considered, the calcium diffusion is better described probabilistically.

Of course, we must also consider the reflection in the boundaries of the subdomain. This effect is taken into account by rejecting those events that result in the positioning of a particle outside the subdomain; in other words, when a particle encounters a wall, we do not move it until the next diffusion time step (in case this further step takes the ion inside the conical subdomain).

The reflection takes place both in the physical upper boundary (cell membrane) as well as in the fictitious walls (lateral side of the cone); reflection in this last case is equivalent to considering that the number of outgoing particles equals that of incoming ones.

Incoming Ca^{2+} current

As previously commented, the value of the whole-cell current I_{wc} is on the order of 100 times the domain current, considering a spherical cell of radius $R = 5$ μm with uniformly distributed calcium channels.

Typically, for a current of $I_d = 10$ pA the number of ions entering the subdomain would be ~400 ions per unit of diffusion time (12.5 μs). Thus, for a density of channels $\rho_{cha} = 15$ channels/μm^2, corresponding to 48 channels for the conical domain, the unitary current will be ~200 fA, corresponding to an approximate number of two ions per channel every 3 μs.

We adopt a simple scheme for simulating the entry of ions. We consider a pulse with a given initial current, typically $I_d = 2$–10 pA in the conical domain, and decreasing exponentially. We take

$$I = I_d^0 e^{-t/\tau}, \quad 0 \le t \le T \tag{2}$$

and $I = 0$ if $t > T$. We will also consider constant pulses.

Among other selections, in our simulation we use the values $I_d^0 = 10$ pA, $\tau = 20$ ms, $T = 50$ ms, which corresponds to a time-averaged current $\langle I_d \rangle = 3.7$ pA and a unitary current of 76 fA, within the range of physiological values (Klingauf and Neher, 1997).

At each simulation time step, the number of incoming ions is evaluated using the exponential (or any another selection), and then the entries are randomly selected from among all available channels. In this way, the number of ions entering through each pore is obtained and the number of free calcium ions in the corresponding compartment beneath the pore is incremented.

This description of the incoming calcium current implies a spatial discretization of the entry points, which, as we have already pointed out, considerably relaxes the assumptions on the symmetry of the distribution of calcium channels. However, it is well known that calcium channels open and close stochastically, so that, for a more realistic description of calcium currents, a discretization in time, considering open/close probabilities for the channels, would be desirable. The time dependence of the calcium current is determined by the variation of the open/close/inactivation probabilities for the calcium channels. Nevertheless, as commented by Klingauf and Neher (1997), channel gating can be expected not to be of importance for the understanding of the (relatively slow) secretory response of neuroendocrine cells. On the other hand, it is likely that fluctuating channels could be important in the study of neurotransmitter release or, in general, in the investigation of rapid responses to calcium signals.

Our Monte Carlo simulation naturally allows a stochastic time description of the calcium current, and as an illustration we will present an example showing the effect of channel gating (see section Channel gating: a simple model).

The opening and closing of calcium channels is modeled as a Markovian process: given the mean open (τ_o) and closed (τ_c) times for the channels, we first select probabilistically the initial state of the calcium channels with probabilities $P_o = \tau_o/(\tau_o + \tau_c)$ of being initially open and $P_c = 1 - P_o$ of being initially closed. Then, for each closed channel we choose the time it will remain closed, using an exponential distribution with expected value τ_c (we proceed similarly with the open channels). After the time for a channel to remain closed has expired, the channel opens and we decide the time it will remain open (and similarly for the transitions open $\rightarrow$ closed).

We are not considering inactivated states; nor are we taking into account the possible variation of the open/closed (and inactivation) times. The study of the dynamics of calcium channels and its dependence on voltage, inactivation by $[Ca^{2+}]$, and so on lies beyond the scope of this work and deserves a separate analysis.

Kinetics

During each diffusional time step Δt and in each compartment of the grid the kinetic equations that describe the buffering processes are applied and the calcium and buffer concentrations evolve. In terms of concentrations, one can describe the first-order kinetics of the process

$$[Ca] + \sum_i [B_i] \rightleftharpoons \sum_i [CaB_i]$$

by the system of equations

$$\begin{cases} \dfrac{d[Ca]}{dt} = \displaystyle\sum_i \{k_-^i[CaB_i] - k_+^i[Ca][B_i]\} \\ \displaystyle\sum_i \dfrac{d[B^i]}{dt} = \dfrac{d[Ca]}{dt}; \quad \dfrac{d[CaB^i]}{dt} = -\dfrac{d[B^i]}{dt} \end{cases} \tag{3}$$

where k_+^i is the forward binding rate for the buffer i and k_-^i is the unbinding rate.

We take the values of the kinetic constants from Klingauf and Neher (1997), except for the endogenous buffer. We only consider two buffering systems (as in Sala and Hernández-Cruz, 1990; Nowycky and Pinter, 1993): an endogenous fixed buffer (500 μM), with the kinetic constants given by Klingauf and Neher (1997), plus an exogenous (and mobile) buffer (Fura-2 or EGTA). Of course, we could have included more buffering systems, but we preferred to keep the model within the minimum number of parameters, given the considerable uncertainties in the kinetic constants for the buffers (in particular for the endogenous buffer(s)).

Because the simulation is performed in terms of the number of ions and buffer molecules, we adopt the first-order kinetic equations in terms of the number of particles of each species in each small cubic compartment of the grid. In terms of the number of free calcium ions N_{Ca}, free buffer

molecules N_{B_i}, and bound buffer molecules N_{CaB_i}, Eq. 3 reads

$$\begin{cases} \Delta N_{Ca} = \sum_i \{\mathcal{K}^i_- N_{CaB_i} - \mathcal{K}^i_+ N_{Ca} N_{B_i}\} \\ N_{CaB_i} + N_{B_i} = N^T_{B_i}; \quad \sum_i N_{CaB_i} + N_{Ca} = N_{Ca^T} \end{cases} \tag{4}$$

where $N^T_{B_i}$ represents the total (free + bound) number of buffer particles of type i, N_{Ca^T} is the total number of calcium ions, and ΔN_{Ca} represents the variation of free calcium ions in a given cubic compartment during a time interval $dt \equiv \Delta t/n$. $\mathcal{K}^i_+$, $\mathcal{K}^i_-$ are defined below.

To integrate the kinetic equations we subdivide the interval Δt into n subintervals of length dt, evaluating probabilistically the changes in the free calcium and the free and bound buffer concentrations for each dt. During the integration of the kinetic equations inside each time interval Δt, the total (free + bound) number of buffer particles of type i and the total number of calcium ions N_{Ca^T} remain constant. These numbers can only change because of diffusion, which is taking place for each Δt ($> dt$).

The effective constants $\mathcal{K}^i_-$ and $\mathcal{K}^i_+$ for binding and unbinding in each time interval dt are given by

$$\mathcal{K}^i_- = k^i_- \frac{\Delta t}{n}; \quad \mathcal{K}^i_+ = k^i_+ \frac{\Delta t}{nV} \tag{5}$$

where Δt is given by Eq. 1, n is the number of subdivisions of the interval Δt used to integrate the kinetic equations, and V is the volume of each cubic compartment.

Starting from the initial conditions for N_{Ca}, N_{B_i}, and N_{CaB_i} and choosing n large enough (dt small enough), one can obtain the final N_{Ca} after each interval dt. Not only the number of calcium ions is required; the changes in the number of free and bound buffer molecules must also be evaluated in each iteration of Eq. 4 and actualized for the next step dt. Because the effects of binding and unbinding for the two buffer species are coupled, the solution to the safe integration of Eq. 4 seems to consist of taking a very small dt and splitting Eq. 4 into different equations for each of the effects (binding-unbinding) and the buffers. Indeed, for small enough dt the small variations due to each of the effects (binding/unbinding) and buffers should have a small impact on the rest. However, given the small number of ions and buffer molecules in each compartment (in particular, the almost nonexistent Ca^{2+} before influx), the variations in each dt could be too small to record any single change when ΔN_{Ca} is considered to be an integer number and finite differences are used to integrate Eq. 4. In fact, using finite differences implies that ΔN_{Ca} (and N_{Ca}, N_{B_i}, etc.) is a real and not necessarily integer number. In other words, ΔN_{Ca}, N_{Ca}, etc., should be interpreted as average values (or expected values); in this way, a macroscopic description in terms of concentrations (Eq. 3) would be equivalent to Eq. 4. However, given the small number of ions and buffer molecules per compartment of the grid, the more straightforward interpretation of N_{Ca}, N_{B_i}, etc., as actual numbers of ions and buffer molecules in a given compartment of the grid is a feasible one.

To implement such a microscopic interpretation, one should describe the system probabilistically, evaluating the probabilities associated with each of the processes and generating events according to such probabilities.

Taking a large enough n one can then split Eq. 4 as follows.

Binding: For each buffer species i one can write the variation in Ca^{2+} ions ($\Delta^i N_{Ca}$) due to binding with such buffer species i as

$$\frac{\Delta^i N_{Ca}}{N_{Ca}} = -\mathcal{K}^i_+ N_{B_i} \tag{6}$$

which in terms of the binding probability means that each Ca^{2+} ion has a probability

$$P^i_b = \mathcal{K}^i_+ N_{B_i} \ll 1 \tag{7}$$

of being bound by any of the N_{B_i} free buffer molecules during the time dt. Such binding probabilities can change after each step dt because the number of free buffer molecules N_{B_i} can vary.

Unbinding: On the other hand, bound buffer molecules can suffer unbinding and increase the number of calcium ions by the amount $\mathcal{K}^i_- N_{CaB_i}$; but this variation equals $-\Delta N_{CaB_i}$, so that

$$\frac{\Delta N_{CaB_i}}{N_{CaB_i}} = -\mathcal{K}^i_-; \tag{8}$$

in other words, each bound buffer particle of type i has a probability

$$P^i_u = \mathcal{K}^i_- \tag{9}$$

of becoming unbound in the interval dt. Notice that the unbinding probability is constant in time, in contrast to the binding probability (arising from the nonlinear terms of the system of equations).

Restrictions: During each diffusional time step, the total number of calcium ions (bound + free) or buffer molecules (bound + free) of each kind is held constant in each compartment.

After evaluating the probabilities of binding or unbinding in a time dt, one can decide the number of ions that undergo any of the processes described. Given a probability p for each ion to be bound (or for a buffer molecule to become unbound), the probability for the binding of k ions of a total of N ions (or unbinding of k buffer molecules of a total of N bound buffer molecules) in a time interval dt is given by the binomial distribution

$$P(k; p, N) = \binom{N}{k} p^k (1-p)^{N-k} \tag{10}$$

Then we can select the number of ions and buffer molecules that become bound or unbound in each time interval dt according to the binomial distribution (for algorithms to generate random deviates that follow binomial distributions, see, for instance, Press et al., 1992, pp. 285–286).

To safely integrate the kinetic equations, a large enough n is selected for every diffusion time Δt. Such a value n is evaluated every time and for each compartment before the kinetic equations are integrated. Therefore, the effective constants $\mathcal{K}^i_-$ and $\mathcal{K}^i_+$ can be different at different time intervals of the simulation, though keeping the same ratio. The selection of the appropriate number of subdivisions of the interval is made by requiring that all binding (and unbinding) probabilities are smaller enough than 1; that is, we set n by bisectioning the interval as many times as required to fulfill the inequalities:

$$\mathrm{Max}(P^i_b, P^i_u) < P_{max}, \quad i = 1, 2 \tag{11}$$

Let us stress that this subdivision is performed locally, both in time (at each diffusion time step) and in space (at each compartment of the grid).

Numerical experiments suggest that $P_{max} = 0.1$ is a safe selection that guarantees proper convergence of the method. Indeed, we do not find any changes in our results by limiting the probabilities by smaller values of P_{max}.

In summary, we have considered that, in each time interval Δt, each bound buffer molecule has a constant probability of becoming unbound while each free calcium ion has a probability of becoming bound, by a given buffer species, proportional to the number of free buffer molecules in a region surrounding the calcium ions (in our simulation, a compartment of the grid). The differential equation (Eqs. 3 and 4) can thus be interpreted as giving statistical averages for the variation of the number calcium ions. In the Monte Carlo simulation we stay at the probabilistic level. The interval Δt is divided into n subintervals d$t = \Delta t/n$ in such a way that all probabilities are small enough. The number of calcium ions that become bound in each interval dt or become unbound is evaluated using the corresponding probabilities and following the distribution in Eq. 10.

The algorithm gives priority to the fastest effects during each Δt (a waiting time can be considered as done when the buffers are diffused). For instance, unbinding is normally so slow that the probabilistic selection of the number of buffer molecules that undergo unbinding can be made at the end of each interval Δt and not necessarily each d$t \leq \Delta t$. In case two or more effects have the same priority in a given time dt, the order in which they act is generated considering equal probabilities for those effects.

Initial conditions

Initially, we consider the number of Ca^{2+} ions and buffer molecules needed to achieve equilibrium for each of the buffer species; in each compartment the condition of equilibrium is given by

$$\mathcal{K}^i_- N_{CaB_i} - \mathcal{K}^i_+ N_{Ca} N_{B_i} = 0 \rightarrow N_{B_i} = \frac{N_{B_i^T}}{(\mathcal{K}^i_+/\mathcal{K}^i_-)N_{Ca} + 1} \tag{12}$$

where N_{Ca} should be understood as the average number of ions in each compartment of the grid. Assuming that the initial concentration of free Ca^{2+} is the basal concentration, $[Ca^{2+}] = 0.1\ \mu M$, which is equivalent to only 310 ions in the whole conical subdomain and 0.07 ions per compartment, Eq. 12 can only be interpreted as giving the average number of free and bound buffer molecules in each compartment. As the expected average number of Ca^{2+} ions in each compartment is by far smaller than 1, locally (in each compartment) there is no possible equilibrium; however, in the whole conical subdomain, equilibrium exists. Of course, because we are following the fate of each ion, there can be one or more ions in each compartment or none at all, but never fractional values.

Regarding the buffers: the typical concentration considered for the fixed endogenous buffer will be 0.5 mM, which, in terms of the number of molecules, means ~350 buffer molecules (free + bound) in each compartment.

These estimations clearly suggest that, at the beginning of a Ca^{2+} pulse, starting from the basal concentration for free Ca^{2+}, there is no way local equilibrium of Ca^{2+} with the different buffer species can be reached in each compartment of the grid. Equilibrium has to be interpreted as an average over the whole conical domain, regardless of how fast the binding/unbinding of each buffer species takes place. Only when the number of Ca^{2+} ions is large enough could local equilibrium possibly be found. Therefore, the assumptions of the rapid buffer approximation (RBA) are not expected to be met on the submicron scale at short times after the beginning of a pulse; however, RBA succeeds in estimating local average concentrations for fast in-mobile buffers, as we will later discuss.

As input data, we consider the basal concentration of calcium and the concentration of the different buffer species as given in Table 1. We distribute the corresponding number of Ca^{2+} ions and buffer molecules (free and bound) randomly and uniformly in the conical subdomain. This is the starting point of our Monte Carlo simulation.

Sequence of the simulation

The sequence of the simulation is carried out as follows.

Presimulation: The number of ions and buffer molecules given by the equilibrium conditions are distributed randomly and uniformly along the conical domain. To ensure that global equilibrium is reached, the distributions of ions and buffers develop during 1 ms according to the kinetic equations; during this presimulation lapse all channels re-

main closed. The system follows its course by means of the same procedures that apply to the actual simulation (except the entrance of ions).

Simulation: For each simulation step, the following actions are taken and repeated in this same order until the end of the simulation.

Entry of ions: The incoming calcium flux is modeled as previously discussed. On most occasions, except when explicitly stated otherwise, the time dependence of the Ca^{2+} is varied continuously according to an exponential decay.

Kinetics: The binding and unbinding are calculated in each compartment, following the previously discussed scheme.

Diffusion of Ca^{2+}: Ca^{2+} ions and mobile buffers are diffused by using the previously discussed random walk scheme. As we mentioned before, diffusion of buffers is delayed with respect to ions, that is, we diffuse the mobile buffers (assuming the ratio of diffusion coefficients is k) after k diffusion cycles have been completed.

RESULTS AND DISCUSSION

In the following, we discuss the effect of the different parameters involved in the simulation. Unfortunately, there is considerable uncertainty as to the actual values of the physical constants describing the endogenous buffers (Klingauf and Neher, 1997; Xu et al., 1997; Naraghi and Neher, 1997). However, our simulation, being valid quite independently of the possible values, can be used safely to study the tendencies when the parameters are varied.

To illustrate the kind of results that can be obtained from our Monte Carlo method, we adopt as standard values those given by Klingauf and Neher (1997) for chromaffin cells. These values, together with the rest of the parameters of the simulation, are summarized in Table 1. We will vary these values to study the effect of the parameters defining the model.

We will show the time courses for free calcium, endogenous (fixed) buffer, and exogenous (mobile) buffer corresponding to short pulses with a duration of 50 ms and different shapes and total currents. Although the simulation is carried out in terms of the numbers of calcium ions and buffer molecules, the results are presented in terms of more easily readable concentrations. However, the fact that we are dealing with a discrete stochastic simulation that moves particles becomes apparent in the dispersion observed when we plot the data generated by the simulation (every 12.5 μs). Each such point corresponds to the concentration at a given time step of the simulation; the number of each type of particle in any given compartment of the grid suffers stochastic fluctuations but gives overall smooth variations when average values are considered. The Monte Carlo simulation not only gives average values for concentrations but also shows the uncertainty of the simulations. The time fluctuations can be interpreted as dispersions in the concentrations when results averaged over time intervals are considered, possibly limited by the temporal resolution of a given experiment (which is expected to be larger than the time step of the simulation).

TABLE 1 Parameters used in the simulation

Geometrical parameters	
Radius	$r = 5\ \mu$m
Length of the grid	$\Delta x = 0.105\ \mu$m
Calcium current parameters	
Incoming current	$I = I_d^0 e^{-t/\tau}\ t \le T$
	$I_d^0 = 10$ pA (*)
	$\tau = 20$ ms (*), $T = 50$ ms
Density of Ca^{2+} channels	$\rho_{cha} = 15\ \mu m^{-2}$ (*)
Kinetic parameters	
Calcium	
Basal concentration	$[Ca^{2+}]_0 = 0.1\ \mu$M
Diffusion coefficient	$D_{Ca} = 220\ \mu m^2/s$
Endogenous buffers	
Total concentration	$[B] = 500\ \mu$M
Forward binding rate	$k_+ = 5 \times 10^8\ M^{-1}\ s^{-1}$ (*)
Dissociation constant	$K_D = 10\ \mu$M (*)
Exogenous Buffer	
Fura-2	
Total concentration	[Fura-2] = 100 μM
Forward binding rate	$k_+ = 5 \times 10^8\ M^{-1}\ s^{-1}$
Dissociation constant	$K_D = 0.24\ \mu$M
Diffusion coefficient	$D_{Fura} = 50\ \mu m^2/s$ (*)
EGTA	
Total concentration	[EGTA] = 1 mM
Forward binding rate	$k_+ = 1 \times 10^7\ M^{-1}\ s^{-1}$
Dissociation constant	$K_D = 0.15\ \mu$M
Diffusion coefficient	$D_{EGTA} = 200\ \mu m^2/s$ (*)

The parameters marked with * are varied in the simulation.

To display our results, we consider two kinds of presentation. The most immediate one consists of directly showing the output of the simulation, with the appearance of scatter plots; the second presentation consists of averaging the time courses (with binning of 10 points) and giving the average value and, eventually, error bars ($2 - \sigma$ confidence level). We choose the first kind of presentation when considering local studies and the second one for showing data averaged over given regions.

Dependence on the intensity of the Ca^{2+} current: saturation levels

Fig. 3 *A* shows the free Ca^{2+} concentrations for the values listed in Table 1 with varying initial domain currents I_d^0 and considering Fura-2 as an exogenous buffer. We consider a current given by Eq. 2, with $\tau = 20$ ms, $T = 50$ ms, and $I_d^0 = 10, 5, 2.5$ pA. Fig. 3, *B* and *C*, shows, respectively, the concentration of free endogenous buffer and exogenous buffer (Fura-2). All of the figures show the averages over the submembrane domain; that is, the results are averages down to $0.105\ \mu m \simeq 100$ nm of depth.

The selection of an exponentially decaying pulse for the simulation is only one possibility among many others. It has

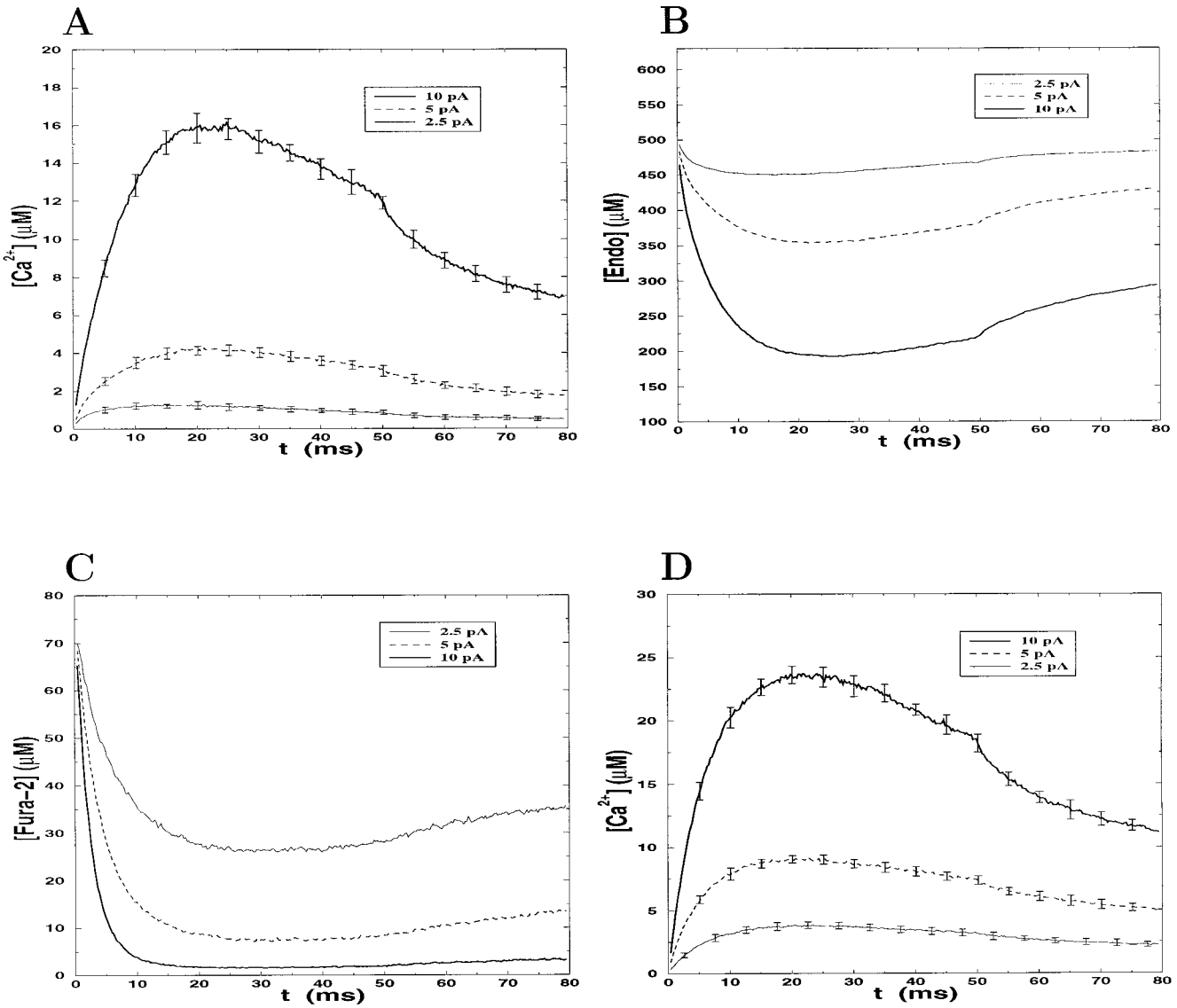

FIGURE 3 Effects of the amplitude of the incoming current on the average concentrations of free calcium and free buffer molecules at depths between 0 and 100 nm. Average values with binning of 10 points, corresponding to time intervals of 10×12.5 μs, are shown. Error bars (2-σ confidence level) for some selected points are displayed for the $[Ca^{2+}]$ time courses; the uncertainties for the buffer time courses are small (lower than 1%), and they are not shown. (*A*) $[Ca^{2+}]$ time course (with 100 μM Fura-2 added) and for three different exponential currents (see Table 1): $I_d^0 = 10, 5, 2.5$ pA. (*B*) Time course for the free endogenous buffer for the same conditions of *A*. (*C*) As in *B*, for the time course of Fura-2. (*D*) As in *A*, without Fura-2.

the theoretical benefit that, as our results will show, the Ca^{2+} concentration near the membrane peaks before the pulse ends. This fact is interesting when different time courses for different kinetic parameters are compared. Constant intensities (as in Sala and Hernández-Cruz, 1990; Nowycky and Pinter, 1993; Klingauf and Neher, 1997) will also be considered.

In Fig. 3 *A* one observes that the free calcium concentration is far from responding linearly when currents in the range of 5–10 pA are considered; in fact, a reduction by a factor of 2 in the incoming current involves a reduction by a factor of 4 in the increase of free Ca^{2+}. This fact can be understood by looking at Fig. 3 *C*: for 10 pA the exogenous buffer saturates rapidly and then the increase in $[Ca^{2+}]$ becomes faster. Under such saturation conditions, the $[Ca^{2+}]$ can be expected to depart from the linearized buffered approximation (Naraghi and Neher, 1997), which assumes low variations of buffer concentrations. For lower currents the response of Ca^{2+} gradually becomes more linear, as can be seen by comparing the rise of $[Ca^{2+}]$ for incoming currents of 5 pA and 2.5 pA; observe also that Fura-2 does not saturate for such currents.

The effect of the exogenous buffer saturation is also shown in Fig. 3 *D*, where the $[Ca^{2+}]$ time course (without

Fura-2) is plotted. As can be seen in the figure, the nonlinear effects shown in Fig. 3 *A* have now become attenuated.

Notice also the steep decrease in free Fura-2 concentration (Fig. 3 *C*), in contrast to the smoother relative variation of endogenous buffer concentration (Fig. 3 *B*). The endogenous buffering system rapidly becomes accommodated to the concentration of free Ca^{2+}, as can be inferred by noticing that $[Ca^{2+}]$ and $[B_{endo}^{free}]$ follow a similar pattern of temporal variation (compare Fig. 3, *A* and *B*); $[B_{endo}^{bound}]$ also demonstrates this pattern (not shown), reaching its maximum when $[Ca^{2+}]$ does. In contrast, the exogenous buffer is not able to keep track of the rapid variation in $[Ca^{2+}]$ (Fig. 3 *C*).

Shape of the Ca^{2+} current

Let us now briefly discuss the importance of the shape of the calcium pulses. Until now, we have chosen an exponentially decaying current as described in Eq. 2, with $\tau = 20$ ms and $T = 50$ ms, which for $I_d^0 = 10$ pA gives a time-averaged current $\langle I_d \rangle = 3.7$ pA. Let us compare such a result with the corresponding one for a constant pulse with a same duration $T = 50$ ms and a same total influx charge; that is, we take $I = 3.7$ pA for $T < 50$ ms, and we switch off the pulse at $T = 50$ ms. The comparison between the result of these two different pulses is shown in Fig. 4, *A* and *B* (considering Fura-2), and Fig. 4 *C* (for EGTA).

Fig. 4 *A* shows the average calcium concentrations, varying in time, for the submembrane domain (0–100 nm). After the pulse has been disconnected, one can observe that the same equilibrium is reached for both the exponential and the constant pulses, which clearly indicates that the same amount of Ca^{2+} ions has entered the cell, and thus the same whole-cell equilibrium has to be reached. However, for the exponential pulse the peak is reached at ~20 ms, while the concentration for the constant pulse (slightly larger in the peak) increases steadily until the end of the pulse (50 ms). The importance of the shape of the macroscopic calcium current becomes manifestly important in determining when the peak is reached and, to a lesser extent, in determining how high the peak is. Of course, as deeper regions are considered (for instance, 300–400 nm, Fig. 4 *B*), the peak for the exponential current is delayed and approaches the peak for the constant current. In any case, for determining concentrations near the membrane a detailed simulation of the calcium current seems to be necessary; not only it is important to know the magnitude of the current, but a good description of the shape of the current is also needed. This will be the subject of further study.

Ca^{2+} concentrations as a function of depth

In Fig. 5 *A*, we can observe the Ca^{2+} concentrations at different depths. Notice how, as expected, the increase in $[Ca^{2+}]$ becomes smaller as the depth grows. In addition, the $[Ca^{2+}]$ peak becomes more delayed as deeper regions are considered. As we go deeper into the cell, the peak of $[Ca^{2+}]$ begins to disappear. In such deep regions, Ca^{2+} ions arrive with considerable delay, and the Ca^{2+} concentration increases steadily to reach the values given by the equilibrium in the whole subdomain.

In Fig. 5 the calcium and free buffer time course for an exponential pulse ($I_d^0 = 10$ pA, $\tau = 20$ ms, $T = 50$ ms) and a total simulated time of 1 s are shown. As can be observed, the concentrations at different depths tend to the same value as the time elapsed becomes longer. Notice, however, that for such "long times" the effect of extrusion of Ca^{2+} should be noticeable. We have not implemented this effect in our simulation because we are mainly concerned with the study of calcium time courses in time intervals on the order of 50–100 ms. The results shown for times of ~1 s, without extrusion, will be used in Appendix A to show that our simulation converges properly at long times. We will show that the final concentrations are in full agreement with the solution of the reaction diffusion problem at long times.

The average values for different depths (Figs. 4 and 5) display the behavior described by Sala and Hernández-Cruz (1990) and Nowycky and Pinter (1993). However, such values are not sufficient to explain the secretory response of cells to calcium influx: as discussed by Klingauf and Neher (1997), the study of submembrane gradients is essential. For such a purpose, the versatility of the Monte Carlo simulation is very useful. We will consider such gradients later. First, let us study the validity of the RBA, focusing on the submembrane domain.

Study of local equilibrium and the RBA hypothesis

Let us consider the following four different kinds of submembrane compartments:

1. Type A: Compartments beneath a channel pore with an extra neighbor pore
2. Type B: Compartments beneath a pore with no extra neighbor pores
3. Type C: Compartments not corresponding to a pore but with a neighbor compartment having a pore
4. Type D: Compartments that have no pore and no neighboring pore

Such characterization of the submembrane compartments enables us to study the local equilibria of the buffering systems with the calcium ions. The percentage deviation from equilibrium of a given species of buffer (i) at given time (and spatial location) reads

$$\mathrm{dev}_i = 100\left(1 - \frac{[B_i]}{[B_i^0]}\right) \tag{13}$$

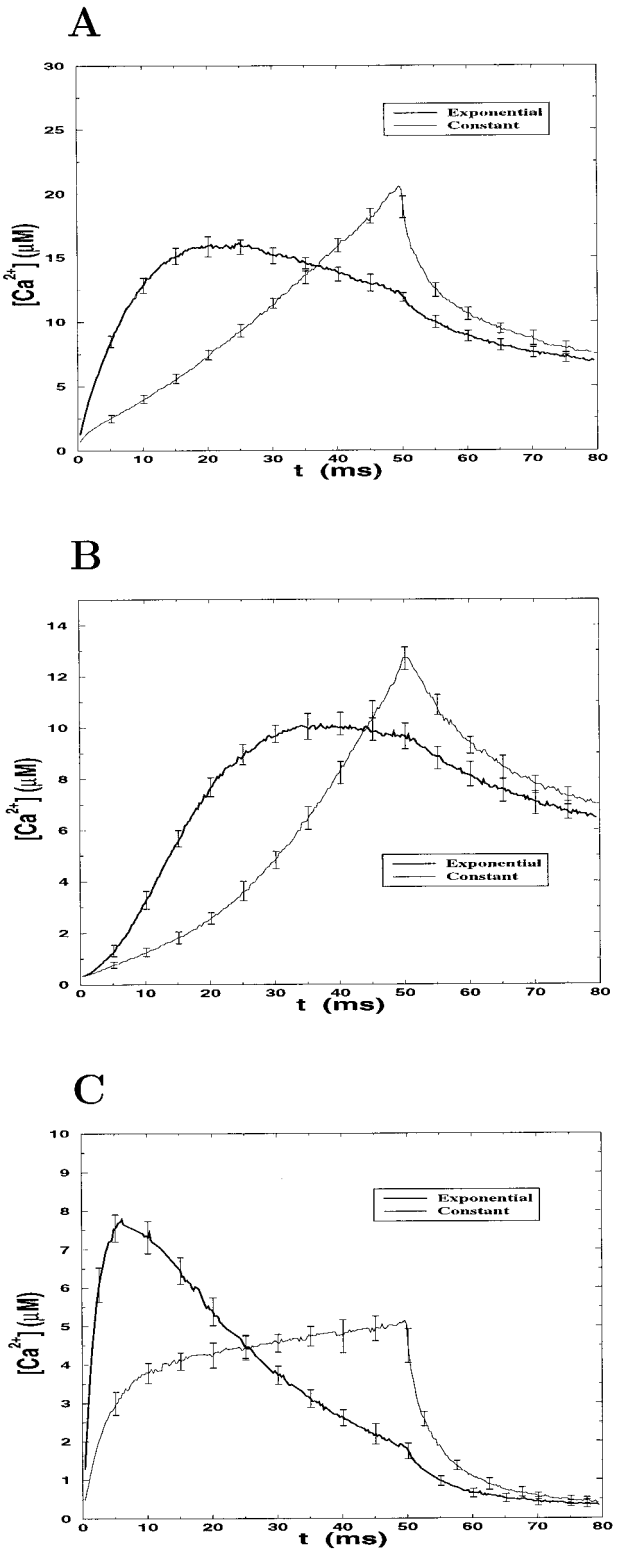

FIGURE 4 Effects of the shape of the current. Average values with binning of 10 points are shown with error bars (2-σ confidence level) for some selected points. (*A*) $[Ca^{2+}]$ time course averaged down to 100 nm of depth, considering an exponentially decaying calcium current and a constant current (Fura-2 added). (*B*) As in *A*, but for depths between 300 and 400 nm. (*C*) As in *A*, but considering EGTA (parameters given in Table 1) instead of Fura-2.

where $[B_i^0]$ is the concentration of free buffer *i* that would be in equilibrium with the calcium concentration [Ca]. By considering the equilibrium equation $k_+[Ca][B_i] - k_-([B_i^T] - [B_i]) = 0$, Eq. 13 can be rewritten in terms of the concentration of free buffer, total buffer, and free calcium. To study the local equilibrium in the different types of compartments ($k = A, B, C, D$), we use Eq. 13 in terms of the number of free calcium ions and buffer molecules:

$$\mathrm{dev}_i^k = 100\left(1 - \frac{N_{B_i}^k}{N_{B_i^T}^k}\left[\frac{\mathcal{K}_+^i}{\mathcal{K}_+^i}\frac{N_{Ca}^k}{N_{com}^k} + 1\right]\right) \qquad (14)$$

where $N_{B_i}^k$, $N_{B_i^T}^k$, and N_{Ca}^k represent, respectively, the number of free endogenous buffer molecules, total (free + bound) endogenous buffer molecules, and free Ca^{2+} ions, summed over all of the compartments of the kind *k* ($k = A, B, C, D$). N_{com}^k is the number of compartments of the type *k*. We apply Eq. 14 to study local equilibrium for both the endogenous buffer and the exogenous buffers; a negative deviation will mean that there is an excess of free buffer molecules.

Fig. 6, *A* and *B*, shows that, regardless of the type of compartment considered, the endogenous buffer reaches equilibrium rapidly and "locally" (but averaging over homologous compartments); this fact suggests that RBA is valid for such a rapid buffer, at least in the average over compartments of the same kind. Notice, however, the dispersion in the plots, which becomes larger as the number of compartments that enter into the average is smaller (A- and B-type compartments). Such stochastic fluctuations will have a larger impact on $[Ca^{2+}]$ concentrations as lower influx currents are considered. Let us stress again that for typical free calcium concentrations of 10 μM an average value of around seven free calcium ions is to be expected in each compartment of the grid; thus, for smaller concentrations there are not enough free calcium ions to meet a stable local equilibrium at scales on the order of 100 nm or smaller. The hypothesis of rapid and local equilibrium for the endogenous buffer is thus seen to be valid as an average over homologous compartments, with typical deviations larger as fewer compartments enter into the average and as lower calcium concentrations and incoming currents are considered. In Appendix B we will discuss how the finding of average local equilibrium of the endogenous buffer is explained by estimating the time the endogenous buffer requires to reach equilibrium, starting from a situation away from equilibrium.

Although equilibrium is reached locally, at least on the average, in general there is no average equilibrium in the whole submembrane domain; this is an effect of the discrete distribution of ion channels that limits the validity of shell models (which assume that Ca^{2+} enters continuously all along the cell membrane). In Fig. 6 *D*, the equilibrium test for the endogenous buffer was performed by counting calcium ions and buffer molecules in the whole first slice of the conical subdomain and for two different currents ($I_d^0 = 10$,

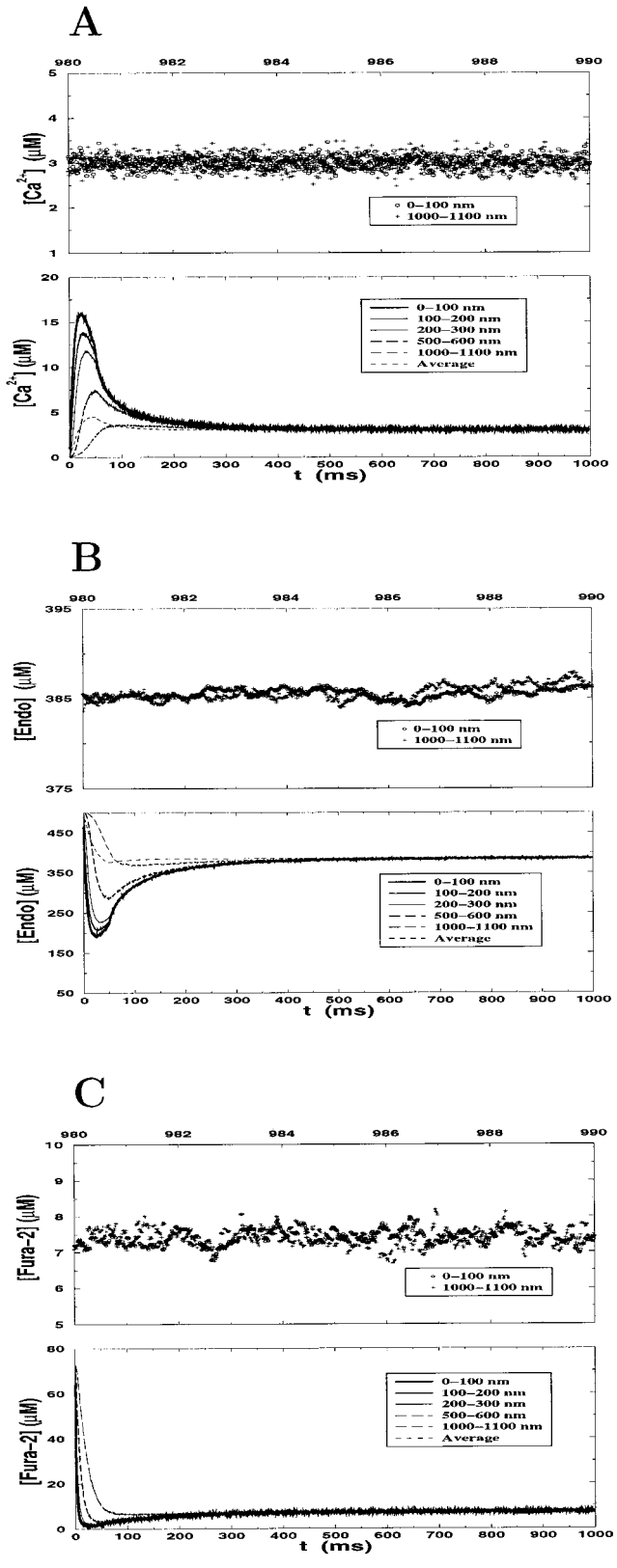

FIGURE 5 Time courses (100 μM Fura-2 added) at different depths (0–100 nm, 100–200 nm, 200–300 nm, 500–600 nm, 1000–1100 nm) for an exponential calcium current lasting 50 ms. A time interval of 1 s is simulated. Averages with binning of 10 points are shown in the bottom-figures, while in the top figures the direct output generated by the simulation is displayed. (*A*) (*Bottom*) $[Ca^{2+}]$ time courses at different depths. The $[Ca^{2+}]$ averaged over the whole conical domain is also shown. As the depth becomes larger the rise in $[Ca^{2+}]$ is smaller and the calcium peak is delayed. (*Top*) detail for long times at 0–100 nm and 1000–1100 nm. (*B*) As in *A*, for the free endogenous buffer. (*C*) As in *A* and *B*, for free Fura-2.

5 pA). The observed displacement is in fact nothing but a manifestation of the $[Ca^{2+}]$ gradients along the submembrane domain (0–100 nm of depth). Such gradients are believed to be fundamental to explain the secretory response of neuroendocrine cells (release-ready granules are located beneath the membrane). Notice that the higher the current the more pronounced the deviation becomes at the beginning of the pulse, which indicates that higher submembrane gradients appear. Later, we will discuss such submembrane gradients in more detail.

In contrast to the endogenous buffer, Fura-2 (with the parameters from Table 1) is not "fast enough" to reach "locally" instantaneous equilibrium. Initially, the exogenous buffer deviates considerably from equilibrium, even in the average over homologous compartments. Such local deviation reflects the fact that Fura-2 (100 μM) has relatively slow kinetics, and it cannot account for all of the incoming calcium current (see Appendix B for more details on equilibration times and the RBA hypothesis). In addition, because Fura-2 is a mobile buffer, bound and unbound Fura-2 can approach the membrane coming from deeper regions, changing the ratio of bound/unbound and hence displacing equilibrium, especially when high $[Ca^{2+}]$ gradients are present. In this way, the mobility of Fura-2 helps to maintain and enhance the deviation of Fura-2 from equilibrium.

It is also worth noting that the kinetics of the endogenous buffer affects the way Fura-2 deviates from equilibrium, as shown in Fig. 6, *E* and *F*. The equilibrium condition is shown for Fura-2; one can observe that displacement from equilibrium changes considerably in the first 10 ms, changing K_D (taking a fixed k_-) for the endogenous buffer. The free Ca^{2+} concentration profiles, of course, become smaller as K_D is taken smaller (not shown). As expected, displacement from equilibrium for Fura-2 persists even when the endogenous buffer is not considered in the simulation (not shown), because, as discussed in Appendix B (see also Naraghi and Neher, 1997), the origin for such a displacement is to be found in the relatively slow equilibration time for Fura-2.

Equilibrium for Fura-2, particularly near the membrane, was shown to depend strongly on the diffusion coefficient. When we performed a simulation considering a buffering system with the same properties as Fura-2, but taking a null diffusion coefficient, we again observed an initial departure from local equilibrium. However, in this case, equilibrium for such a buffer was reached in less than 2 ms in the presence of endogenous buffer (not shown).

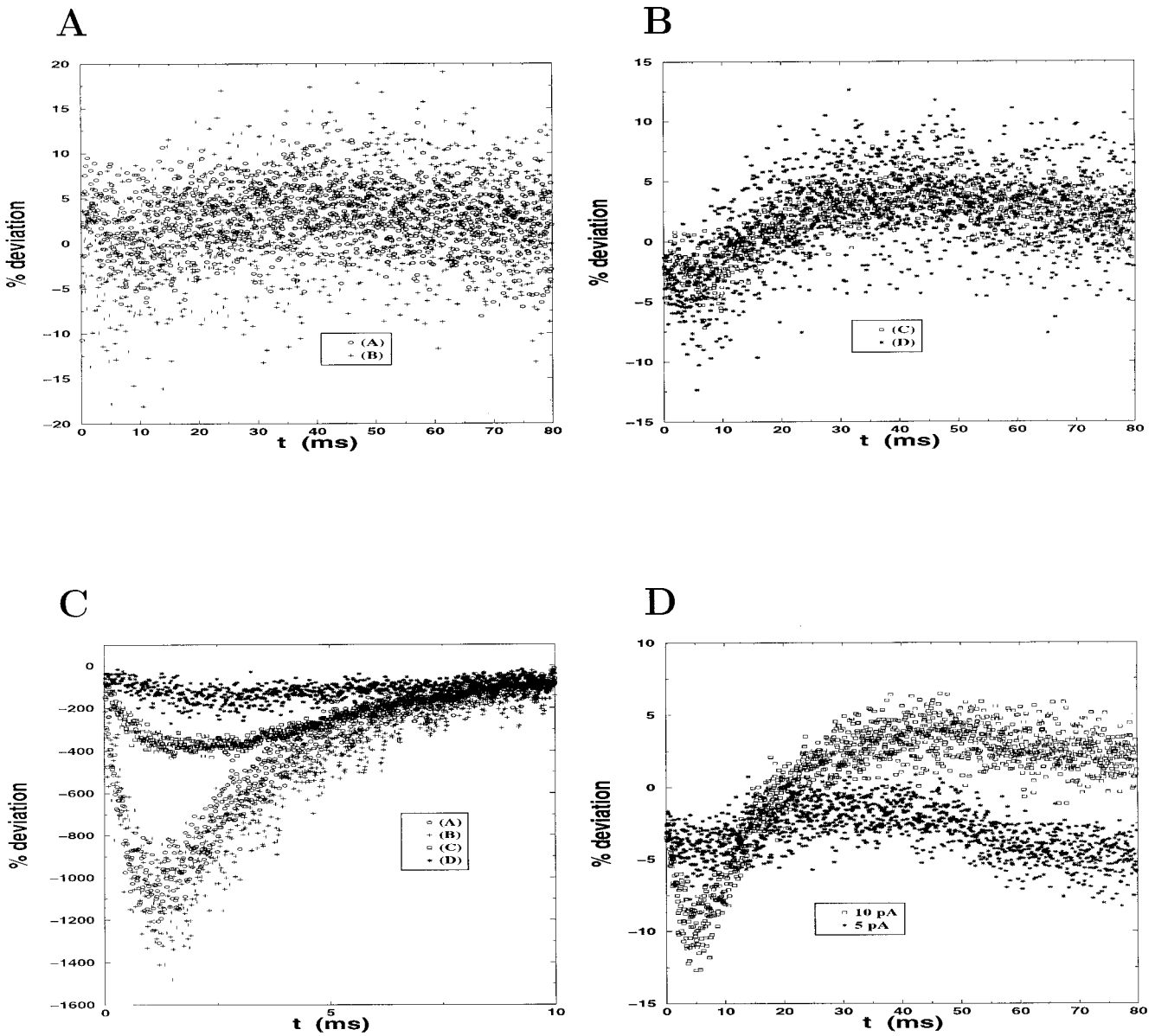

FIGURE 6 Tests of equilibrium for the endogenous buffer as well as for Fura-2 (100 μM). For every 10 steps of simulation the output given by the simulation is plotted. (*A*) Deviation from equilibrium (in %) for the endogenous buffer for $I_0 = 500$ pA and Fura-2 (100 μM) added; the equilibrium is tested both for A-type and B-type compartments (see text). (*B*) As in *A*, for compartments of type C and D. (*C*) Percentage deviation time course of the exogenous buffer (Fura-2) with the conditions of *A* and *B*. The deviation is tested for compartments of type A, B, C, and D; the largest deviations occur for the compartments nearest the channels (A and B compartments, which are almost indistinguishable in the figure); the deviation for C-type is larger than for D-type. (*D*) Percentage deviation from equilibrium of the endogenous buffer as an average at depths between 0 and 100 nm. Two incoming currents are considered: $I_d^0 = 10$ pA (largest deviation at small ts) and $I_d^0 = 5$ pA. (*E*) Deviation from equilibrium for Fura-2 in the first 15 ms of the pulse for compartments of type B and two choices of the endogenous buffer kinetic parameters: $k_+ = 5 \times 10^8$ M^{-1} s^{-1}, $K_D = 10$ μM, and $k_+ = 1 \times 10^8$ M^{-1} s^{-1}, $K_D = 50$ μM. The largest deviation occurs as k_+ becomes larger (k_- is the same in both cases). (*F*) As in *E*, for compartments of type C. (*G*) Percentage deviation time course of EGTA for compartments of type A, B, C, and D. For A and B compartments the deviation is the largest and the plots overlap; the smallest deviation is for D compartments.

Regarding EGTA, because this buffer is slower than Fura-2 (see Appendix B) and it has a considerably larger mobility, even more deviation from local equilibrium is expected, as indeed happens (Fig. 6 *G*). Considering a buffer with the same properties as EGTA (Table 1) but with a zero diffusion coefficient, we can see in Fig. 7 *D* (as happened with Fura-2 with the same change) that the initial displacement from equilibrium is much smaller and has a smaller duration compared to the real case in which EGTA moves. It becomes clear that mobility is acting against local

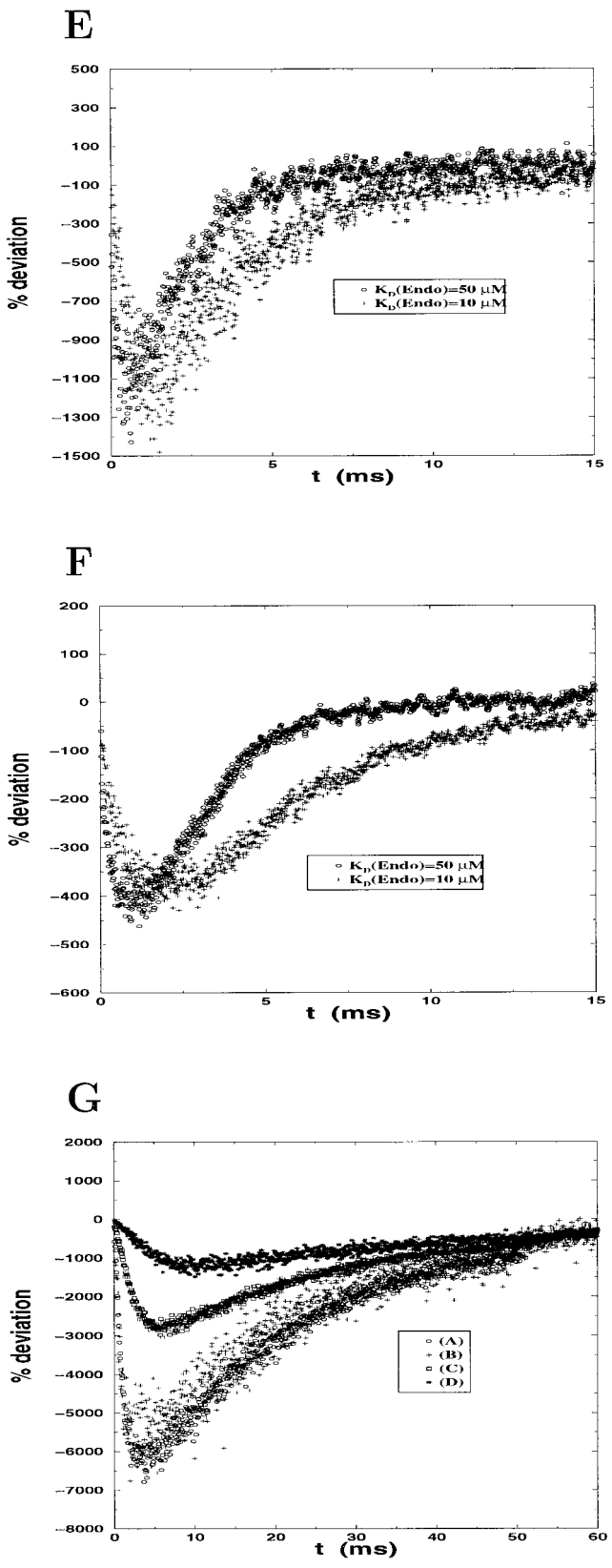

FIGURE. 6 Continued.

equilibrium when concentration gradients are present; such an effect is, of course, more important, as the buffer considered has slower kinetics.

Notice how EGTA approaches saturation levels when a zero diffusion coefficient is assumed (Fig. 7 *C*). When EGTA is forced to be fixed in the simulation, no unbound EGTA can approach, and, given the small K_D and k_- for EGTA, it rapidly saturates near membrane.

Given that exogenous buffers are used as indicators of $[Ca^{2+}]$, the departure from equilibrium of exogenous buffer concentrations indicates that the measurement of $[Ca^{2+}]$ in fluorescence experiments (assuming equilibrium of such buffer with calcium) could grossly underestimate the actual free calcium concentration (as suggested by Smith et al., 1996). Indeed, the equilibrium test is displaced to negative values, which shows that there is less exogenous bound buffer than expected from equilibrium. Such displacement is related to the previously discussed "blindness" of both Fura-2 and EGTA to the calcium time course (Nowycky and Pinter, 1993).

Mobility of buffers

In Fig. 7, *A* and *B*, the effect of the mobility of buffers on the $[Ca^{2+}]$ time course can be observed.

In Fig. 7 *A*, we consider the choice of parameters from Table 1 for Fura-2 and the possibility of having a buffer with the same parameters as Fura-2, except that its diffusion coefficient is taken to be approximately equal to the coefficient for calcium; the calcium peak is then observed to be lower as the diffusion coefficient is taken to be larger. This reflects the fact that Fura-2 can now transport calcium to other regions much more rapidly because the diffusion coefficient is larger. The effect of considering higher mobilities is then to produce a more rapid washing out of the regions of high Ca^{2+} concentration. In Fig. 7 *B*, we repeat the simulation, but now for EGTA (with the values of Table 1). We also consider the possibility of having immobile EGTA (zero diffusion coefficient), to show the effect of mobility. As before, the calcium peak becomes smaller as the mobility is higher.

As previously discussed, the mobility of buffers has a considerable impact on the ratio of unbound to bound buffer molecules, especially when high concentration gradients are present (as happens at the start of the pulse). The relatively slow exogenous buffers (Fura-2, EGTA) show larger deviations from local equilibrium at the beginning of the pulse as their mobility is taken higher (Fig. 7 *D*). Notice, furthermore, that this fact can affect the saturation levels of the buffer (Fig. 7 *C*). Thus, if the mobility of exogenous buffers was restricted in cytoplasm, the time course of the free buffer could change considerably in the submembrane region, where high gradients appear.

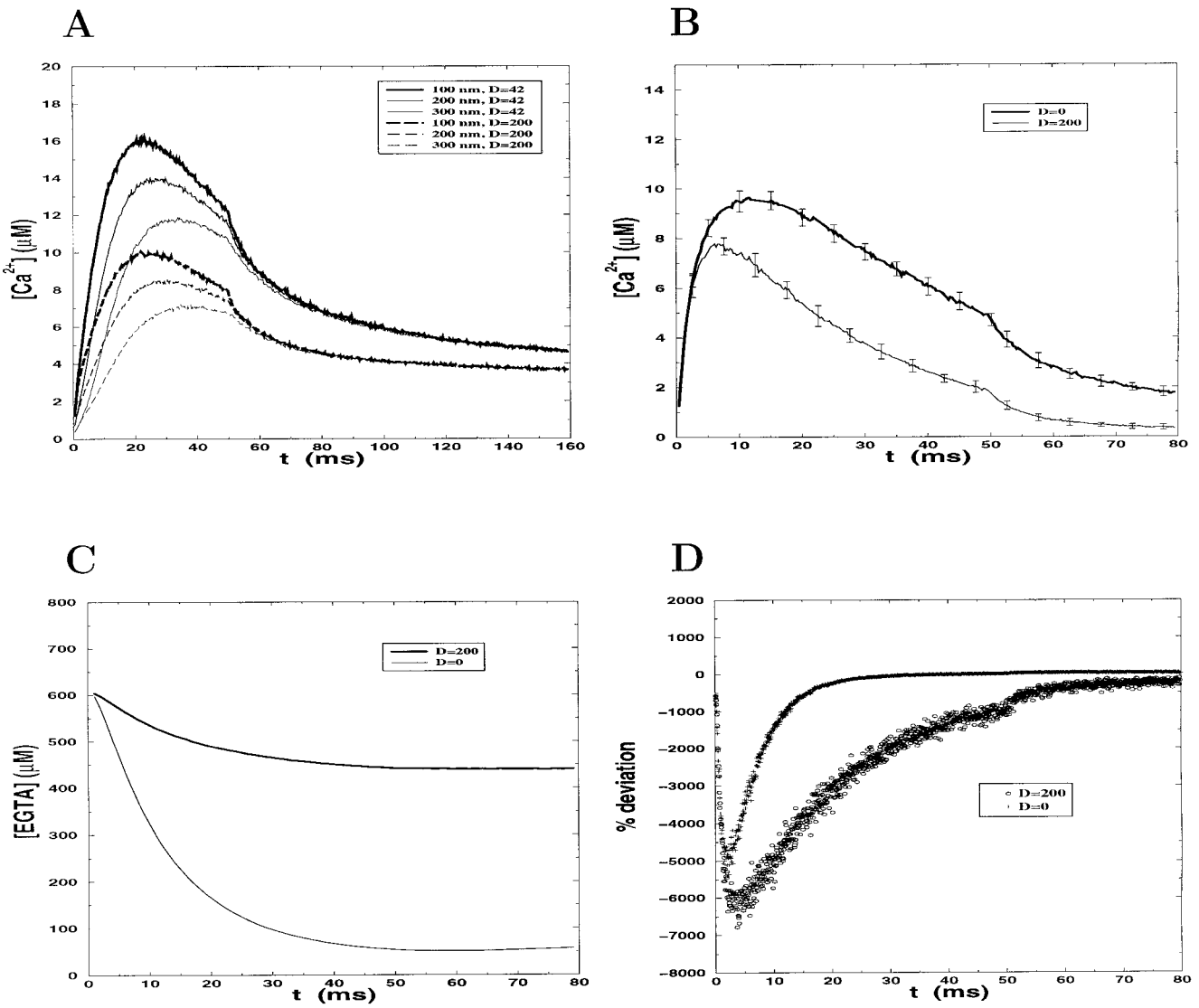

FIGURE 7 Effects of the diffusion coefficient of buffers; averages with binning of 10 points are shown, except in *D*. (*A*) Averaged $[Ca^{2+}]$ time course considering two different diffusion coefficients for Fura-2 ($D_{\text{Fura-2}} = 42\ \mu m^2/s$ and $D_{\text{Fura-2}} = 200\ \mu m^2/s$) at different distances from the pores (*from top to bottom*: 0–100 nm, 100–200 nm, 200–300 nm). The uncertainties are similar to those displayed in Fig. 3 *A*, and they are not shown here. (*B*) $[Ca^{2+}]$ time course averaged over the submembrane domain (0–100 nm), considering two diffusion coefficients for EGTA: $D_{\text{EGTA}} = 200\ \mu m^2/s$ and $D_{\text{EGTA}} = 0\ \mu m^2/s$. (*C*) As in *B*, for the concentration of free EGTA. (*D*) Percentage deviation time course for free EGTA, considering the diffusion coefficients of *B* and *C*. The test of equilibrium is performed over A-type compartments; the points plotted correspond to the output of the simulation (every 10 steps).

Submembrane $[Ca^{2+}]$ gradients and dependence on the density and distribution of calcium channels

As was previously suggested (Klingauf and Neher, 1997), submembrane gradients depend on the density and distribution of channel pores. One of the advantages of our Monte Carlo simulation lies in the easy and natural implementation of the entry of calcium ions through channel pores and the flexibility with which one can distribute the calcium channels over the membrane. On the contrary, the solution of differential equations can be a hard task when the boundary conditions do not show some regularity or symmetry; besides, there exists the intrinsic difficulty of describing discrete entries for the calcium ions when continuous quantities (as concentrations) are being considered. Such a difficulty becomes even greater if one wishes to discretize the entry of calcium in time, that is, if one wants to consider the probabilities of the opening and closing of the channels. A Monte Carlo simulation is able to deal with such situations. However, although in reality channels open and close stochastically, it is believed that this is not a major effect in neuroendocrine cells (see Klingauf and Neher, 1997). Notwithstanding, examples will be given for a simple model of stochastic opening and closing of calcium channels.

At this stage, we keep to a continuous time description of the calcium current and a discrete spatial treatment of the influx that copes with different distributions of channels, regularly distributed or not.

Let us now study the $[Ca^{2+}]$ time courses, both as an average over the submembrane domain (depth 0–100 μm) and at different locations in such subdomain. Let us consider an incoming current given by Eq. 2 with $I_d^0 = 10$ pA; thus, the time-averaged current per channel will be 76 fA for a density of channels $\rho_{cha} = 15\ \mu m^{-2}$ (48 channels). Fura-2 (100 μM) will be the exogenous buffer.

Different distributions of channels with different densities, keeping the total current fixed, will be taken into account. Together with the selection of our standard (Table 1) value $\rho_{cha} = 15\ \mu m^{-2}$, we will consider $\rho_{cha} = 5\ \mu m^{-2}$, corresponding to 16 channels. In this last case, the unitary current through each pore will be three times bigger. This last distribution can also be interpreted as a distribution of small groups of three channels, clustered in regions smaller than $0.105 \times 0.105\ \mu m^2$, with a unitary average current 76 fA through each of the 48 channels. We also consider the possibility of having the 48 channels clustered in groups of four channels, giving rise to 12 clusters; we place each of the four channels for each cluster in squares of side 2×0.105 μm (one channel in each of the four compartments forming such square). In all cases we distribute the location of the channels or channel clusters randomly and uniformly along the membrane of our conical domain, checking that the resulting distributions are statistically representative and approximately uniform. We do not allow overlapping of channels or clusters (notice, however, that the case $\rho_{cha} = 5\ \mu m^{-2}$ corresponds to the overlapping of three channels in a region smaller than $0.105 \times 0.105\ \mu m^2$).

Fig. 8 *A* shows the $[Ca^{2+}]$ time course, averaged over the submembrane domain, corresponding to $\rho_{cha} = 15\ \mu m^{-2}$ and $\rho_{cha} = 5\ \mu m^{-2}$. Notice that the $[Ca^{2+}]$ time course averaged over the submembrane domain is very similar in the two cases. When the distribution of 12 channel clusters is considered, the resulting averaged $[Ca^{2+}]$ is very similar and lies between the two curves in Fig. 8 *A* (not shown). As a result, the average submembrane concentrations do not depend crucially on the distribution of calcium channels, which validates the use of radial models (Sala and Hernández-Cruz, 1990; Nowicky and Pinter, 1993) to evaluate such averages.

However, for the different types of submembrane compartments (Fig. 8, *B* and *C*), the differences in the $[Ca^{2+}]$ time course are evident when $\rho_{cha} = 15\ \mu m^{-2}$ (48 entries) with $\rho_{cha} = 5\ \mu m^{-2}$ (16 entries) are compared, not surprisingly, because, for a same total current, the Ca^{2+} current through each entry is larger when fewer entries are considered. As can be seen, the more pores a compartment has in its neighborhood, the higher the $[Ca^{2+}]$ peak is at the compartment; besides, the $[Ca^{2+}]$ is delayed when the compartment is located further off the pores, similar to what happened when we considered averages at different depths.

From now on, let us interpret the case $\rho_{cha} = 5\ \mu m^{-2}$ as the result corresponding to small clusters of three channels. When compared with the time course for $\rho_{cha} = 15\ \mu m^{-2}$ (in particular for B compartments), it becomes evident that $[Ca^{2+}]$ beneath each of these clusters cannot be obtained by adding the $[Ca^{2+}]$ due to each isolated pore. This fact indicates that the system is far from being in a linear regime (Naraghi and Neher, 1997). Such failure of the superposition principle can also be observed by comparing the calcium time course for compartments A in Fig. 8 *D* with the time course for compartments B in Fig. 8 *B*. Indeed, the free calcium concentrations are smaller than those obtained by summing the separate effects of the different channels forming the cluster.

Further information can be obtained by comparing the time courses for the three different distributions of channels. First, let us observe that for A-type compartments the calcium peak is higher for higher local concentrations of channels. The same is true for type B compartments (however, there are no B compartments in the case of four-channel clusters). Notice also (Fig. 8, *B* and *C*) that for each distribution of channels, the calcium time course is very similar for A-type and B-type compartments, and, in fact, such time courses are almost indistinguishable in Fig. 8 *C*. This means that the $[Ca^{2+}]$ in each compartment having a pore (or several pores) depends mainly upon the current entering into such compartments through the membrane and depends little upon the entrance of ions through pores that are at neighbor compartments (at an average distance of 100 nm). In other words, the endogenous buffering system has enough capacity to buffer most calcium ions within distances of ~100 nm because it is still relatively far from saturation (on the contrary, Fura-2 totally saturates before 10 ms below the pores in all of the cases shown). The slight difference between type A and B in Fig. 8 *B* (the difference unobservable for Fig. 8 *C*) is related to fine details of the configuration of channels. For $\rho_{cha} = 15\ \mu m^{-2}$ (Fig. 8 *B*) A-type compartments having two or more neighbor A compartments are quite probable, while for $\rho_{cha} = 5\ \mu m^{-2}$ such configurations are infrequent and indeed do not happen in our configuration; all A-type compartments happen to have only one neighbor A compartment.

Interestingly, the similarity between A-type and B-type $[Ca^{2+}]$ time courses would drastically alter if the endogenous buffer system approached saturation below the pores. This effect can be observed when three-channel clusters (for $\rho_{cha} = 5\ \mu m^{-2}$) appear in three neighbor type-A compartments, resulting in a total of nine channels in three neighbor compartments (not shown). The free endogenous buffer falls below 50 μM at the calcium peak for such compartments, and the concentration for A channels almost doubles that appearing in Fig. 8 *C* (not shown).

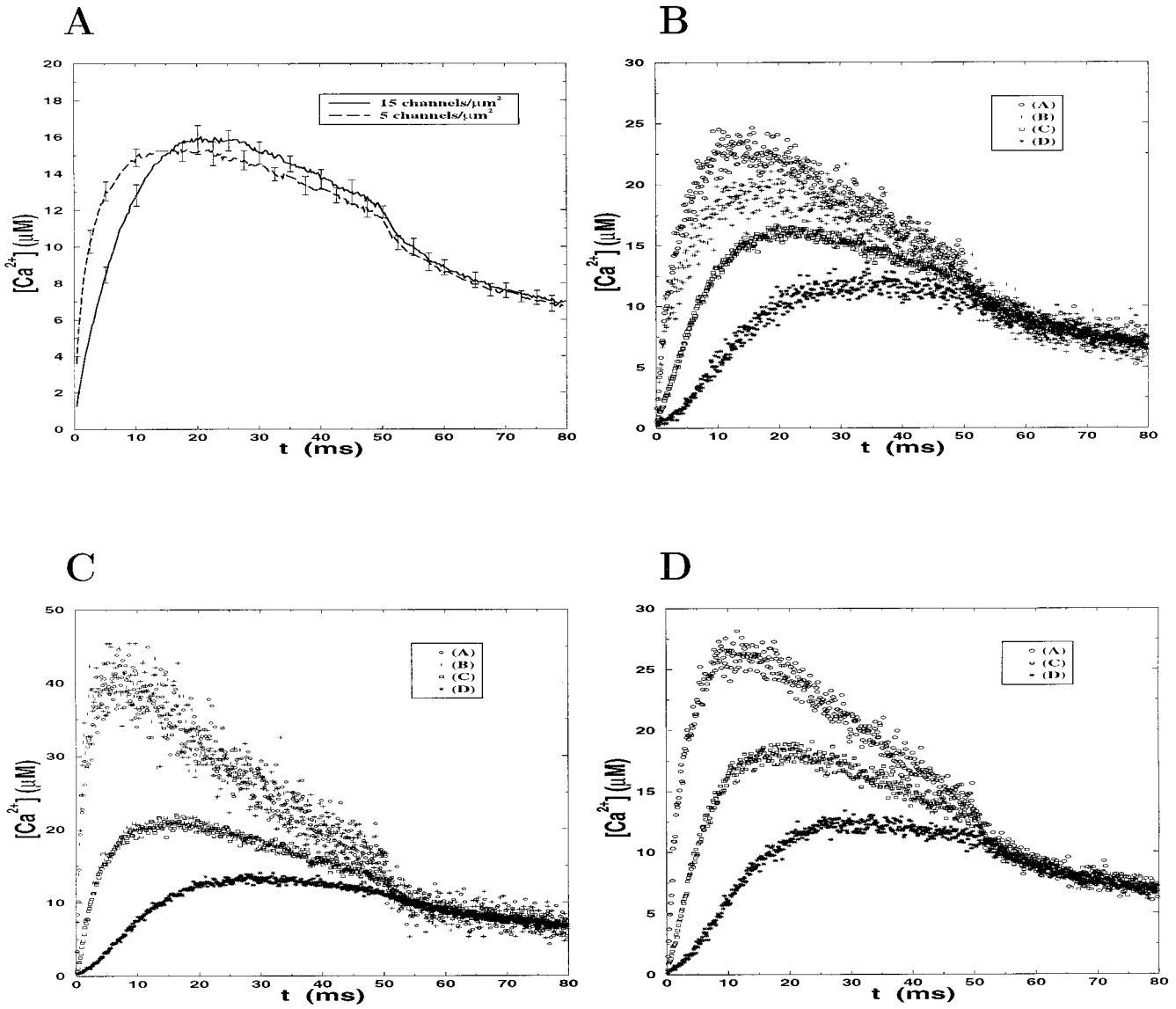

FIGURE 8 Effect of the density of channels. (*A*) Averaged $[Ca^{2+}]$ time course (0–100 nm) for $\rho_{cha} = 5$ channels/μm^2 and $\rho_{cha} = 15$ channels/μm^2 (average values with binning of 10 points are shown). The $[Ca^{2+}]$ plot for $\rho_{cha} = 5$ channels/μm^2 peaks slightly before that for $\rho_{cha} = 15$ channels/μm^2. (*B*) $[Ca^{2+}]$ time course at compartments of type A, B, C, D (from higher to lower concentrations) and $\rho_{cha} = 15$ channels/μm^2. In this figure, as well as in *C* and *D*, we show the direct output of the simulation each 10 steps of simulation. (*C*) As in *B*, for $\rho_{cha} = 5$ channels/μm^2. A and B compartments are indistinguishable in this case. (*D*) As in *B*, but for clusters of four channels (see text). In this case there are no B-type compartments.

When comparing the C-type calcium time courses in Fig. 8, *B*, *C*, and *D*, we again observe that the peak is higher as the clusters have a greater concentration of channels; however, the difference between the different types of clusterization is smaller than for the case of A and B compartments. The difference between C-type and A,B-type is thus larger as the degree of clusterization becomes higher. This means that, as expected, the submembrane gradients become higher as the channels are more concentrated in clusters.

With respect to D-type compartments, observe that the $[Ca^{2+}]$ time courses in Fig. 8, *B*, *C*, and *D*, are very similar. The calcium concentrations at distances larger than 200 nm from the pores depend very little on the actual distribution of channel pores; however, it is clear that for $\rho_{cha} = 5\ \mu m^{-2}$ there will be D compartments farther away from any pore than for the case $\rho_{cha} = 15\ \mu m^{-2}$. The concentration is liable to fall to lower values and with higher gradients, starting from higher values near the pores, as the degree of clusterization increases. However, the overall values in the submembrane domain are very similar in all cases (Fig. 8 *A*).

Channel gating: a simple model

Finally, let us briefly discuss the effect of the stochastic opening and closing of channels as an illustration of the

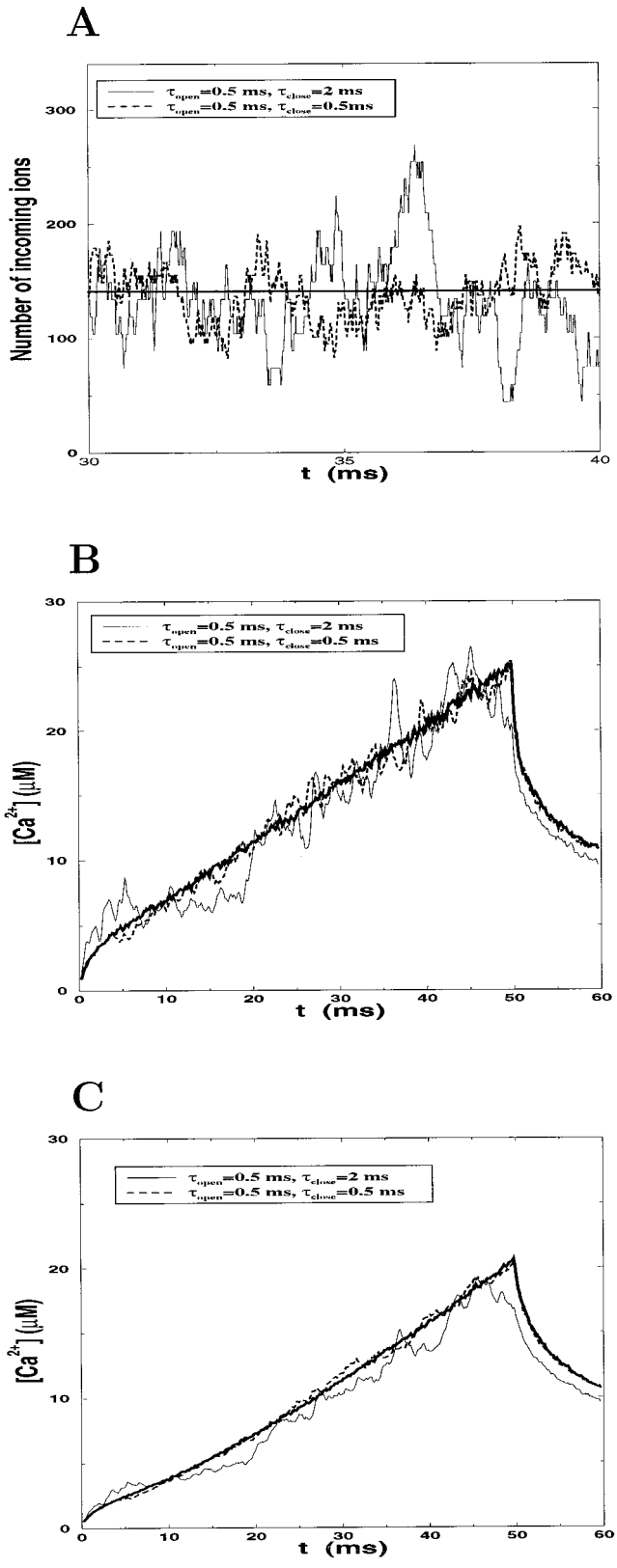

FIGURE 9 Effects of the opening and closing of channels; we show the averages with a binning of 10 points. (*A*) Number of incoming ions during each simulation time step (12.5 μs) for three different selection of average open and closed times: τ_{open} = 0.5 ms and τ_{close} = 2 ms; τ_{open} = 0.5 ms and τ_{close} = 0.5 ms; all channels open (τ_{close} = 0). (*B*) [Ca^{2+}] time course at compartments of type A for the parameters of *A*. (*C*) As in *B*, for the average over the submembrane domain (0–100 nm).

potential of our model. As discussed by Klingauf and Neher (1997), the opening and closing of channels is not expected to be of great relevance for secretion in chromaffin cells, and the same is expected to be true for pancreatic β-cells. However, although probably beyond the scope of the present paper, we will show how one can, quite naturally, take into account the stochastic character of the calcium current. It is believed that the modeling of this effect can be of importance in neurotransmitter release (Yamada and Zucker, 1992), and future efforts will be in that direction.

The opening and closing of calcium channels is modeled, as we explained before, as a Markovian process. A simple simulation consisting of two-state (opened/closed) channels with constant mean open and close times is considered. Results will be shown for a mean open time τ_o = 0.5 ms and for two different selections of the closing time τ_c = 0.5 ms and τ_c = 2 ms, which seem to be within the range of physiological values for L-type calcium channels (Smith et al., 1989). As before, we consider a density of channels ρ_{cha} = 15 μm^{-2}, and we distribute the channels randomly and uniformly. The unitary currents per channel and unit time are fixed in such a way that their average over the duration of the pulse is, approximately, 76 fA. That is, the unitary current for the constant pulse is 76 fA, and for the fluctuating current with $\tau_c = \tau_o$, the unitary current is 2 × 76 fA during the time a channel remains open, while for $\tau_c = 4\tau_o$ the unitary current is 5 × 76 fA. In this way, one can compare the [Ca^{2+}] time course for the constant pulse (Fig. 4 *A*) with 10 pA for the whole conical domain with the time courses when opening and closing channels are considered. Let us consider a calcium pulse lasting 50 ms.

In Fig. 9 *A* we have a sample (from 30 to 50 ms) of the calcium currents in the three cases studied; the number of incoming ions (in the whole conical domain) per unit of diffusion time is shown as a function of time. The currents for τ_c = 0.5 ms and τ_c = 2 ms fluctuate around the constant current, showing that approximately the same number of calcium ions enter the cell during the calcium pulse. As expected, for τ_c = 0.5 ms the current fluctuates more rapidly than for τ_c = 2.0 ms. Higher peaks are reached for τ_c = 2.0 ms because a higher unitary current is considered in this case to have a similar time-averaged current.

As can be seen in Fig. 9 *B*, the calcium time course for τ_c = 0.5 ms oscillates around the values corresponding to the constant current more rapidly than in the case of the simulation for τ_c = 2 ms. In addition, given that for τ_c = 2 ms the current reaches higher peaks than for τ_c = 0.5 ms, the calcium time course shows larger departures from the value for the constant pulse for τ_c = 2 ms. We can see that

for the spatiotemporal resolution of our simulation, the effect of opening and closing channels is to produce transient deviations from the simpler modeling of calcium influx consisting of a uniform distribution of ions over the randomly distributed entries.

In Fig. 9 *C* we compare the free calcium concentration time courses, averaged down to 100 nm of depth, for the three cases described. The average values show, as expected, that the fluctuations are softened as larger spatial domains are considered. The main noticeable effect is that the Ca^{2+} concentration for $\tau_c = 2$ ms lies below the one corresponding to the constant pulse and that, correspondingly, the decline after the pulse is switched off is different. This effect is due to the fact that, although the total incoming calcium should be similar for the two cases, because of the probabilistic nature of the opening and closing, they are not necessarily equal. In other words, the difference between the result for the constant pulse and the pulse with $\tau_c = 2$ ms is due to the finite size of our system, which consists of 48 channels and a relatively short (50 ms) fluctuating current.

The differences in the total number of incoming calcium ions would be smaller (fixing the unitary currents to have the same time-averaged unitary current) if the pulse lasted a longer time T and then τ_o/T, τ_c/T became very small, if the number of channels was larger, or in the case where τ_c became much smaller than τ_o; in connection with this, notice that the difference with respect to the constant pulse is smaller for the case where $\tau_c = 0.5$ ms.

It is important to stress again that the results shown correspond to a particular spatial distribution of channels and to a particular stochastic calcium current. By performing several simulations, with different random sequences for the Ca^{2+} current, we observed, as expected, that the number of simulations with $\tau_c = 2$ ms that gave average (0–100 nm) calcium time courses above the constant current $[Ca^{2+}]$ time course tends to be equal to the number of simulations below it. Furthermore, the peaks and valleys observed change their position and intensity for different randomly selected spatiotemporal configurations.

CONCLUDING REMARKS

We have modeled 3-D buffered diffusion of calcium ions, using a random walk algorithm and a probabilistic interpretation of the kinetic reactions. This is a safe interpretation, even for low calcium currents and concentrations, and thus seems appropriate for a microscopic description of the 3-D buffered diffusion under physiological conditions.

Such a scheme enables us to study the influence of the kinetic, diffusional, and geometrical parameters of the model, considerably relaxing the assumptions about the symmetry of the system that have been considered so far. The flexibility of the simulation allows us, for instance, to study submembrane calcium gradients for different configurations of channels that are not necessarily regularly distributed. In addition, the incoming calcium currents can be discretized in time in such a way that channels open and close with given probabilities. An example of such stochastic description has been given that can serve in the future to analyze the calcium transients in the vicinity of calcium channels for realistic descriptions of channel dynamics.

Our method has enough generality to serve as a test for other previous approximations, not necessarily in the context of spherical neuroendocrine cells. For instance, we have checked that radial (shell) models are appropriate for describing average calcium concentrations in the submembrane domain, at least for regions of 100 nm thickness. We have also studied local equilibrium of the buffering systems to test the RBA hypothesis (rapid buffering approximation), and we have investigated the nonlinearity of the response to calcium influx (testing the linearized buffering approximation).

Conclusions that can be drawn from our simulations are as follows.

1. There is a highly nonlinear response of free $[Ca^{2+}]$ at buffer saturation levels; the response becomes more linear as the buffers are farther from saturation. For the typical Fura-2 concentration (100 μM), such a buffer is seen to saturate in the submembrane region for domain currents on the order of 10 pA.
2. The different shapes of the free calcium time course for different shapes of the macroscopic incoming currents with the same total influx of Ca^{2+} suggest that a detailed modeling of physiological calcium influxes can be important in understanding the secretory response of neuroendocrine cells.
3. For the standard values given by Klingauf and Neher (1997), the endogenous buffer time course closely follows the shape of the free $[Ca^{2+}]$ time course. This is related to the fact that RBA for the endogenous (and immobile) buffer considered here is a reasonable approximation, at least as an average. However, both Fura-2 and EGTA (slower than the endogenous buffer and mobile) are rather blind to the calcium time course. Given that exogenous buffers are used as indicators of $[Ca^{2+}]$ in fluorescence experiments, this relative "blindness" can be of experimental relevance, given that the assumption of equilibrium usually considered will lead to an underestimation of $[Ca^{2+}]$. Because the displacement from equilibrium increases as the mobility becomes higher, slowly moving buffers seem preferable.
4. The increase in $[Ca^{2+}]$ due to a number of clustered channels cannot be obtained by adding the effect of the different (isolated) channels. Thus the superposition principle is not valid in general, and the free calcium concentration below a cluster of N channels is smaller than N times the increase in $[Ca^{2+}]$ below one isolated channel.

5. Larger free Ca^{2+} concentrations are found near the ion pores, with steeper gradients in the submembrane domain as the density of channels is taken to be smaller for the same macroscopic (domain) current. When the channels form clusters, the gradients become steeper and the calcium concentrations near the clusters become higher as more channels are clustered in a smaller region. However, the $[Ca^{2+}]$ time course, averaged over the submembrane region, is similar regardless of the existence of clusters. Furthermore, the calcium time course averaged over the submembrane regions at distances larger than 200 nm from the nearest pores is similar for different clusterizations. Thus the effect of the presence of clusters can affect the secretory response mainly when the distribution of secretory granules is correlated with the distributions of calcium channels and clusters. Clusters could facilitate secretion, given the appearance of higher calcium concentrations near them. On the other hand, nonclustered channels could give rise to a higher total number of free calcium ions near the channel pores. As a consequence, clusterization would be efficient for secretion by the granules near the pores if a relatively high threshold has to be surpassed to trigger secretion. A contrary situation of no clusters would be more interesting in a scenario where secretion by the granules near the pores increases with total increasing free calcium below the pores and the threshold to trigger secretion is low. The possible advantage of clusterization fades away at distances from the cluster larger than 200 nm.

APPENDIX A: PERFORMANCE AND VALIDATION OF THE MONTE CARLO CODE

Our Monte Carlo code, written in Fortran 77, was run in a SUN Enterprise 3000 computer. For a run of 80 ms, the program typically spends 45 min, depending on the parameters of the simulation. The program requires moderate computational and storage requirements and can be run on a personal computer. In a PC with a Pentium II (350 MHz) processor, an 80-ms simulation can be performed in ~2 h and 15 min.

The different modules of the program have been both separately and jointly validated. The main subroutines of the program are the subroutine for 3D diffusion and the subroutine for the kinetics of the buffering system. The subroutine for 3D diffusion was tested by checking that free diffusion of particles (initially at a given compartment of a grid) resulted in Gaussian distributions for each of the spatial dimensions, with widths correctly given by the diffusion coefficient and the elapsed time. The algorithm for simulating kinetics was tested for different values of the kinetic constants and different initial concentrations by checking that equilibrium was reestablished starting from concentrations far from equilibrium, and that once it is reached, the equilibrium is stable.

For the full simulation, several validations were taken into account. Among them are the following.

The gradients due to the discrete spatial distribution of entry channels becomes less noticeable as deeper regions are considered, and the concentration profiles tend to those predicted by shell models. The fast and fixed buffering systems are found to be in local equilibrium with Ca^{2+}, while the exogenous buffers are displaced from equilibrium at the start of a pulse; this displacement is expected from qualitative arguments (see Appendix B). The concentrations after the end of the pulse tend to the same equilibrium values for any shape of pulse with the same total incoming number of calcium ions.

We have performed additional tests to check that the code converges properly at long times. We have performed simulations lasting 1 s for different buffering systems and different calcium currents. In Fig. 5, the results are given for a 1-s simulation consisting of an exponential pulse of 50 ms duration with 100 μM Fura-2 added. We have checked that the concentrations of total calcium (free + bound) and total buffer molecules are consistent with the initial conditions, and the incoming current and the concentrations given by the simulations at 1 s agree with what is expected from the equilibrium conditions once all gradients have disappeared.

The total concentration of calcium (free + bound) in the whole conical domain ($[C_T]$) at the end of the pulse is easily obtained by adding to the initial concentration of total calcium (obtainable from the initial concentration of free calcium $[Ca^{2+}] = 0.1$ μM and from the equilibrium condition with buffers) the contribution given by the integration of the incoming calcium current. For the parameters of the simulation shown in Fig. 5, this calculation gives $[C_T] = 219$ μM, in full agreement with the simulated result (218.5 μM).

The concentration of free calcium at long times can be obtained by considering that, because of diffusion, all gradients will have disappeared, and then the system will be in global equilibrium. Indeed, we observe in Fig. 5 that the different average concentrations for the free calcium [Ca] at different depths converge to the same values at long times; the same is true for the concentrations of free (or bound) buffers. Because $[C_T]$ is a constant of movement (after the end of the pulse), the global equilibrium at long times implies that

$$[C_T] = [Ca]\left(1 + \sum_i \frac{[B_i^T]}{K_D^i + [Ca^{2+}]}\right) \qquad (15)$$

where [Ca] is the concentration of free Ca^{2+} in equilibrium with the buffers $i = 1, 2, \ldots$, with total (fixed) concentrations $[B_i^T]$ and dissociation constants K_D^i.

For the case shown in Fig. 5, the solution of the third-degree equation (Eq. 15) for $[Ca^{2+}]$ gives the real solution $[Ca] = 3.1$ μM, in agreement with the simulated result at long times. By using the equilibrium equations it is straightforward to verify that the concentrations of free and bound buffers are also correctly given by the simulation.

We have considered this kind of numerical check for different buffering systems and for different calcium currents. With all of these tests, we have full confidence in the correct performance of our algorithms.

APPENDIX B: ON TIME SCALES AND RBA

It is tempting to compare our results for the deviation from equilibrium near the calcium channels with the time-scale hypothesis of RBA (Wagner and Keizer, 1994), which serves to estimate the range of validity of such approximations.

As discussed, RBA assumes that each buffering system is in local equilibrium with calcium. Thus it is reasonable to think that RBA is a good approximation when the characteristic times for the kinetic reaction of Ca^{2+} with the buffers are much smaller than the characteristic times for diffusion. A key point then is to conveniently define such time scales.

To obtain a time scale for the kinetic reactions, let us consider the kinetic equations for a single buffering system:

$$\frac{d[Ca]}{dt} = -k_+[Ca][B_i] + k_-([B_i^T] - [B_i]) \qquad (16)$$

and let us define a new variable α such that

$$[Ca] = [Ca^o] - \alpha; \quad [B_i] = [B_i^0] - \alpha \qquad (17)$$

where $[Ca^o]$ is the calcium concentration in equilibrium with a free buffer concentration $[B_i^o]$. Substituting Eq. 17 in Eq. 16 and considering the equilibrium relation for $[Ca^0]$ and $[B_i^o]$, we have

$$\alpha(t) = \alpha(0)e^{-t/\tau^e} \tag{18}$$

where $\alpha \ll [B_i^T] + K_D$, with $\tau^e = k_+B_i^T + k_-$. This means that, if the system is perturbed from equilibrium, it will come back to equilibrium after a time on the order of τ^e (provided the deviation is not large enough to oversaturate the buffer). Then we can call τ^e the equilibration time and use it as the characteristic time for the kinetics.

Notice that to obtain such a characteristic time a single perturbation from equilibrium (α) has been considered; furthermore, we have considered only one buffer species.

For our selection of the kinetic parameters the following equilibration times for the three buffering species considered are obtained:

$$\tau^e_{endo} \simeq 4\ \mu s, \quad \tau^e_{Fura\text{-}2} \simeq 20\ \mu s, \quad \tau^e_{EGTA} \simeq 100\ \mu s$$

Such characteristic times explain the observed deviation from equilibrium at the start of the pulse for compartments below the pores. At the start of the exponential pulse, with an initial domain current $I_d^0 = 10$ pA, around eight calcium ions enter through each of the channels for each simulation time step (12.5 μs), and the initial average number of ions per compartments is as low as 0.07; thus, for equilibrium to be instantaneously established before the next simulation time step, the buffering system should act on time scales smaller than such a time step. This is the case for the endogenous buffer; however, the kinetics for Fura-2 (and EGTA) is not rapid enough to reestablish equilibrium every 12.5 μs. Moreover, it is reasonable to think that this deviation from equilibrium will increase in time at the start of the pulse until the average number of free calcium ions per compartment becomes at least comparable with the number of incoming ions per simulation step, so that the deviation from equilibrium caused by the incoming current becomes relatively smaller. This is indeed the case, as can be seen from Fig. 6: one can observe that the RBA hypothesis below the pores is met for the endogenous buffer while the same does not hold for the exogenous buffers considered; as expected, the deviation is greater as the incoming current is increased. This suggests that, to estimate whether local equilibrium will be met below the pores, the time scale for equilibration should be compared with a certain time scale associated with the incoming current. It is also reasonable to consider that, at the start of the pulse and below the pores, such characteristic times for the incoming current are of greater relevance than the diffusional time scale that we are discussing next.

The third type of time scale that comes into play is the diffusional time scale. Provided that we consider local equilibrium in a region were no Ca^{2+} sources are present (or they are of low intensity), we are left with two types of scales that can serve to decide whether local equilibrium can be met: the equilibration time scale defined above and the diffusional time scale.

The diffusional time scales can be defined by considering the diffusion coefficient for a given species (Ca^{2+} or mobile buffers) and combining it with a characteristic length scale L, depending on the gradients of the system, to give:

$$\tau^D = L^2/D \tag{19}$$

Local equilibrium of a buffering system will hold as long as $\tau^D \gg \tau^e$, meaning that the variations in the concentrations due to diffusion are much slower than those caused by the kinetic reactions with buffers. L can thus be thought of as being a characteristic distance defined in such a way that the diffusion of calcium ions (and/or mobile buffer) from a distance L to the point in consideration would change the equilibrium relation significantly. Clearly, such a characteristic distance not only depends on the gradients of the system but also on the kinetics of the system and degree of saturation of buffers, because, for example, the same increase in Ca^{2+} due to diffusion can give rise to a considerably different free Ca^{2+} after the calcium undergoes buffering (depending, for instance, on the degree of saturation of buffers). For this reason a precise definition of the length scale appears to be rather difficult to achieve.

As a reference, let us take L to be equal to the length of the grid; this could serve to test equilibrium at C-type compartments (compartments not having a pore but with a neighbor pore), in the (reasonable) belief that the main source for deviation from equilibrium would the presence of a pore, at an average distance to the nearest pore equal to the length grid. In this case ($L = 105$ nm) we get

$$\tau^D_{Ca} \simeq \tau^D_{EGTA} \simeq 50\ \mu s, \quad \tau^D_{Fura\text{-}2} \simeq 250\ \mu s$$

Considering the fastest characteristic diffusion time (for Ca^{2+}) to be the most relevant, we observe that $\tau^e_{Fura\text{-}2}$ is not much smaller than τ^D, and the situation is even worse for EGTA. Thus local equilibrium for Fura-2 and EGTA cannot be reached in the submembrane compartments of type C when high submembrane gradients are present (especially at the beginning of the pulse). In fact, there is displacement from equilibrium in any type of submembrane compartment. The amplitude of the initial displacement is observed to be smaller as larger depths are considered.

AG and JS thank Dr. F. Sala and Dr. S. Sala for carefully reading the manuscript and for enlightening discussions. The authors thank Dr. E. Andreu for useful comments. Two of the authors (AG and JS) acknowledge the hospitality of CWI (Amsterdam), where part of this work was done.

BS acknowledges financial support from the Ministerio de Educación y Ciencia under project PM98-0105 and from the EC under project PI96-3055.

REFERENCES

Allbritton, N. L., T. Meyer, and L. Stryer. 1992. Range of messenger action of calcium ion and inositol 1,4,5-triphosphate. *Science.* 258:1812–1815.

Augustine, G. J., M. P. Charlton, and S. J. Smith. 1985. Calcium entry and transmitter release at voltage clamped nerve terminals of squid. *J. Physiol. (Lond.).* 367:163–181.

Bokvist, K., L. Eliasson, C. Ämmälä, E. Renström, and P. Rorsman. 1995. Co-localization of L-type Ca^{2+} channels and insulin-containing secretory granules and its significance for the initiation of exocytosis in mouse pancreatic B-cells. *EMBO J.* 14:50–57.

Chow, R. H., J. Klingauf, C. Heinemann, R. S. Zucker, and E. Neher. 1996. Mechanisms determining the time course of secretion in neuroendocrine cells. *Neuron.* 16:360–376.

Chow, R. H., L. von Rüden, and E. Neher. 1992. Delay in vesicle fusion revealed by electrochemical monitoring of single secretory events in adrenal chromaffin cells. *Nature.* 356:60–63.

Clapham, D. E. 1995. Calcium signaling. *Cell.* 80:259–268.

Eliasson, L., E. Renström, W.-G. Ding, P. Proks, and P. Rorsman. 1997. Rapid ATP-dependent priming of secretory granules precedes Ca^{2+}-induced exocytosis in mouse pancreatic β-cells. *J. Physiol. (Lond.).* 503:399–412.

Klingauf, J., and E. Neher. 1997. Modeling buffered Ca^{2+} diffusion near the membrane: implications for secretion in neuroendocrine cells. *Biophys. J.* 72:674–690.

Kruk, P. J., H. Korn, and D. Faber. 1997. The effects of geometrical parameters on synaptic transmission: a Monte Carlo simulation study. *Biophys. J.* 73:2874–2890.

Llinás, R., Z. Steinberg, and K. Walton. 1981. Relationship between presynaptic calcium current and postsynaptic potential in squid giant synapse. *Biophys. J.* 33:323–351.

Naraghi, M., T. H. Müller, and E. Neher. 1998. Two-dimensional determination of the cellular Ca^{2+} binding in bovine chromaffin cells. *Biophys. J.* 75:1635–1647.

Naraghi, M., and E. Neher. 1997. Linearized buffered Ca^{2+} diffusion in microdomains and its implications for calculation of [Ca^{2+}] at the mouth of an open channel. *J. Neurosci.* 17:6961–6973.

Neher, E. 1998. Vesicle pools and Ca^{2+} microdomains: new tools for understanding their roles in neurotransmitter release. *Neuron.* 20: 389–399.

Nowycky, M. C., and M. J. Pinter. 1993. Time courses of calcium and calcium-bound buffers following calcium influx in a model cell. *Biophys. J.* 64:77–91.

Ölveczky, B. P., and A. S. Verckman. 1998. Monte Carlo analysis of obstructed diffusion in three dimensions: application to molecular diffusion in organelles. *Biophys. J.* 74:2722–2730.

Press, W. H., S. A. Teukolski, W. T. Veterling, and B. P. Flannery. 1992. Numerical Recipes in Fortran, 2nd Ed. Cambridge University Press, Cambridge.

Riley, M. R., H. M. Buettner, F. J. Muzzio, and S. C. Reyes. 1995. Monte Carlo simulation of diffusion and reaction in two-dimensional cell structures. *Biophys. J.* 68:1716–1726.

Sala, F., and A. Hernández-Cruz. 1990. Calcium diffusion modeling in a spherical neuron. *Biophys. J.* 57:313–324.

Saxton, M. J. 1994. Anomalous diffusion due to obstacles: a Monte Carlo study. *Biophys. J.* 66:394–401.

Saxton, M. J. 1996. Anomalous diffusion due to binding: a Monte Carlo study. *Biophys. J.* 70:1250–1262.

Smith, P. A., P. Rorsman, and F. M. Ashcroft. 1989. Modulation of dihydropyridine-sensitive Ca^{2+} channels by glucose metabolism in mouse pancreatic β-cells. *Nature.* 342:550–553.

Smith, G. D., J. Wagner, and J. Keizer. 1996. Validity of the rapid buffering approximation near a point source of calcium ions. *Biophys. J.* 70:2527–2539.

Wagner, J., and J. Keizer. 1994. Effects of rapid buffers on Ca^{2+} diffusion and Ca^{2+} oscillations. *Biophys. J.* 67:447–456.

Xu, T., M. Naraghi, H. Kang, and E. Neher. 1997. Kinetic studies of Ca^{2+} binding and Ca^{2+} clearance in the cytosol of adrenal chromaffin cells. *Biophys. J.* 73:532–545.

Yamada, W. M., and R. S. Zucker. 1992. Time course of transmitter release calculated from simulations of a calcium diffusion model. *Biophys. J.* 61:671–682.